Analysis of Braided Composites Structures and Yarns for Compression Loading and Design for First Bending Mode

by

Shivacharan Sekhar Mysore

A Thesis submitted to the Graduate Faculty of
Auburn University
in partial fulfillment of the
requirements for the Degree of
Master of Science

Auburn, Alabama
August 16, 2017

Keywords: Braiding, O-ACS, Composites, Compressive Strength, Modal Analysis

Approved by

David Beale, Chair, Professor of Mechanical Engineering
Royall Broughton, Jr., Professor Emeritus of Polymer and Fiber Engineering
Winfred A. Foster, Jr., Professor Emeritus, Aerospace Engineering

Abstract

The open architecture composite structures team at Auburn University has developed prototypes of strong, ultra-lightweight braided lattice structures for primary application in the aerospace sector.

This research focuses on experimentally finding the compression failure loads of a 48K-core braided carbon-fiber composite cord-preg yarn #6. Different compression test fixtures such as Spherical-end, Hex-end, Cap-nut-end fixtures were designed and developed for testing the yarn specimen. Specimens of yarn #6 with varying span-lengths in the range of 7 mm to 90 mm were experimentally tested for compressive strength and the loads at which buckling occurred were found to be in span-lengths exceeding 35 mm. The results of this work provide design parameters for structures with yarn #6 to improve the axial and helical yarn count, helical angle and span-length of axial yarns in the structure.

Finite element analysis was used to find the 1st bending frequency of the largest OACS tubes designed and manufactured by the Auburn University team and its potential application as an RF transparent antenna support on communication satellites. Finite Element (FE) models of small OACS tubes with 45 mm diameter and 300 mm length, and full-scale OACS tubes with 250 mm diameter and 900 mm length were designed to exceed 100 Hz., 1st bending frequency - a design requirement for the satellite application. The modelling involved, OACS tubes with all-carbon yarns, all-glass yarns and carbon-glass hybrid structures. Effects of changes to the geometrical shapes such as conical and cylindrical OACS tubes on the full-scale models have also been studied. This study concludes that an OACS tube 250 mm in diameter and 900 mm in length with the set design and boundary conditions will achieve the design requirement of 1st bending mode of 100 Hz., and this will be achieved by using, a 4 mm diameter all-carbon-fiber yarn architecture (approximately 324K carbon tows) comprising of, 48 axial yarns, 8 clockwise helical and 8 counter-clockwise helical yarns with a 45 degree braid angle.

Acknowledgements

I am grateful to have the constant support and encouragement from my family and friends; I am ever indebted to you all.

Thanks to Dr. Beale, Dr. Broughton and Dr. Foster for introducing me this wonderful research work and guiding me through this journey.

Thanks to the OACS research team for all the support and work they have put into the research, Austin G., Nakul K., and Uday S., Yang Shen, Sanyam S., have all shared valuable knowledge and I thank them for lending a helping hand whenever I needed it the most.

Thanks to Dr. Suhling and Dr. Mishra for believing in me and all the professors who've helped me grow as an engineer and as a person during my time at Auburn.

Table of Contents

Chapter 1 Introduction 1

1.1 Carbon Fiber Composites 1

1.2 Composite Fabrication Using Carbon Fibers 2

1.3 Composite Braiding Manufacturing Process 4

1.3.1 Braiding Process Flow 5

1.3.2 Tow Preg 5

1.3.3 Braiding Tow Pregs Into Yarns 6

1.3.4 Braiding OACS Tubes 6

Chapter 2 Braided Yarn Compression Testing and Failure Modes 8

2.1 Introduction and Scope of Work 8

2.2 Braiding and Curing of Cordpreg for Compression Test 9

2.3 Design and Development of Yarn - Compression Test Fixtures and Specimen 10

2.3.1 Spherical Compression Test Fixture 11

2.3.2 Cylindrical Flat-End Hole Compression Test Fixture 13

2.3.3 Cap-Nut End Compression Test Fixture 14

2.3.4 Hex-End Compression Test Fixture 15

2.4 Compression Loading of Yarn #6 at Different Span-lengths 17

2.5 Yarn #6 Comparisons 21

2.6 Conclusions from Compression Testing of Yarn#6 23

2.7 Compression Breaking Load Prediction of Carbon Fiber Braided Yarn #6 Using Statistical Linear Regression Analysis 24

2.7.1 Conclusion 32
Chapter 3 OACS as an Optical Tube on NASA's IROC Satellite 33
3.1 Introduction and Scope of Work 33
3.2 Compressive Stiffness Test of OACS Structures 36
3.3 FE-Modal Analysis on All-Carbon-Fiber and All-Glass-Fiber OACS 39
3.4 Modeling and Boundary Conditions of the OACS Tubes 40
3.4.1 Initial Test Sample 44.45 mm Diameter 300 mm Long, All-Carbon-Fiber OACS 46
3.4.2 OACS All-Carbon-Fiber Modal Results 46
3.4.3 Initial test sample 44.45 mm diameter 300 mm long – All-Glass-Fiber OACS 47
3.5 OACS Experimental Modal Survey - NASA Glenn - Ref. [6] 49
3.5.1 Boundary Condition – Experimental Modal Analysis 50
3.5.2 Accelerometer Placement 51
3.5.3 Modal Excitation – Impact Hammer Drive Point Locations 52
3.5.4 Data Acquisition Setup & Processing 52
3.5.5 Test Methodology 53
3.5.6 Conclusion 55
Chapter 4 FE Analysis to Find 1st Bending mode of Full Scale OACS Tube 56
4.1 Scope of work 56
4.1.1 Naming Convention of OACS Tubes 57
4.2 FEA of Tapered or Conical OACS for IROC Application 58
4.2.1 Equal Diameter Axial and Helical Yarns – 12x6x6 OACS Tube 59
4.2.2 Larger Diameter Axial Yarns Compared to Helical Yarns – 12x6x6 OACS 61

4.3 FEA of Cylindrical OACS for IROC Application 63
4.3.1 48x12x12x60D all 4 mm Diameter Yarns 63
4.3.2 48x8x8x45D All 4 mm Diameter Yarns 64
4.3.3 48x12x12x45D All 4 mm Diameter Yarns 65
4.3.4 Design for RF transparency 66
4.3.5 Visualization of Wireframe - OACS Boundary Conditions and Results 67
4.3.6 Cylindrical OACS FE-Modal Analysis Results 69
4.4 Conclusion 71
Bibliography 72
Appendix 73
6.1 fell_point Matlab Parameters to Generate OACS Tube Coordinate Points 73
6.2 Consolidating Generated Coordinate Points for ANSYS APDL 75
6.3 ANSYS APDL FEA Input-File Generation Code 76
6.4 Toray T700s Specification 78
6.5 Toray T300 Specification 78
6.6 Yarn #6 Specification Sheet 79
6.7 OACS Tubes End Caps for 44.5 mm Diameter x 300 mm Long 80

List of Figures

Figure 1.1: Surface area-to-volume ratio A/V of a cylindrical particle of given volume plotted vs. particle aspect ratio a = l/d 1
Figure 1.2: Hand lay-up composite fabrication 2
Figure 1.3: Spray-up composite fabrication 2
Figure 1.4: Compression molding 3
Figure 1.5: Filament winding process 3
Figure 1.6: OACS Braiding Process 4
Figure 1.7: OACS Manufacturing Process Flow 5
Figure 1.8: Carbon Fiber Tow, Toray T700s 5
Figure 1.9: Braided tow preg (yarn) 6
Figure 1.10: Braiding OACS tubes 6
Figure 2.1: Yarn Compression testing flow chart 8
Figure 2.2: Braiding of Yarn #6; Photograph from [2] 9
Figure 2.3: Yarn #6 - Oven Curing 10
Figure 2.4: Spherical Groove Compression Test Fixture 11
Figure 2.5: Spherical End Compression Test Specimen 12
Figure 2.6: Spherical-end compression test method 12
Figure 2.7: Cylindrical Flat-End hole compression test method 13
Figure 2.8: Cap-Nut compression test method 14
Figure 2.9: Hex End compression test specimen 15
Figure 2.10: Hex End Yarn #6 compression test specimens 15
Figure 2.11: Hex-end compression test method 16
Figure 2.12: Axial yarn Span-length in OACS 17
Figure 2.13: Compression test specimen – yarn #6 19
Figure 2.14: Compression loading of braided yarn #6 19
Figure 2.15: Brittle-fracture and Buckling failure 20

Figure 2.16: C/S of yarn #6 with jacket 21
Figure 2.17: C/S area of yarn #6 core w/o jacket 21
Figure 2.18: Euler Curve [5] 21
Figure 2.19: Yarn #6 - compressive stress vs. slenderness ratio 22
Figure 2.20: Yarn span-length 24
Figure 2.21: Experimental data 25
Figure 2.22: Fit plot for maximum compression load, ‘y’ 31
Figure 2.23: Residual for maximum compression load, 'y' 32
Figure 3.1: Schematic of IROC Satellite, reprinted from [6] 33
Figure 3.2: IROC-OACS process flow 35
Figure 3.3: Compression Test process flow 36
Figure 3.4: OACS Specimen 36
Figure 3.5: OACS tube under compression 37
Figure 3.6 Stiffness Comparison of OACS tubes 38
Figure 3.7: Carbon fiber OACS – Cantilever Boundary Condition 39
Figure 3.8: ANSYS APDL OACS FE Model 40
Figure 3.9: ANSYS APDL Element specification 41
Figure 3.10: BEAM element mesh of the OACS in ANSYS APDL 43
Figure 3.11: Modelling of Aluminum flange - Boundary condition 44
Figure 3.12: FE Modelling of end mass 44
Figure 3.13: OACS Mass measurement for FE modelling 45
Figure 3.14: Mode 1 – lateral bending all-carbon- fiber OACS tube (Cantilevered Condition) .. 46
Figure 3.15: Glass-fiber OACS 47
Figure 3.16: Mode 1 lateral bending all-glass-fiber OACS tube (Cantilevered Condition) 48
Figure 3.17: Experimental Modal IROC-OACS test specimen 49
Figure 3.18: Modal Test fixture; reprinted from [6] 50
Figure 3.19: Accelerometer mounting; reprinted from [6] 51
Figure 3.20: Impact hammer drive point location; reprinted from [6] 52

Figure 3.21: Data Acquisition; reprinted from [6] 52
Figure 3.22: All Tubes, 90° Drive Point Location, Test Orientation 1, 1st Resonance Frequency Grouping; reprinted from [6] 54
Figure 4.1: FE process flow, IROC-OACS 56
Figure 4.2: FEA naming convention 57
Figure 4.3: Tapered OACS with equal core diameter yarns 59
Figure 4.4: Tapered OACS with larger axial yarn diameter 61
Figure 4.5: Cylindrical IROC - 48x12x12x60D 63
Figure 4.6: Cylindrical IROC - 48x8x8x45D 64
Figure 4.7: Cylindrical IROC - 48x12x12x45D 65
Figure 4.8: "Gap" requirements for RF transparency 66
Figure 4.9: Modal Analysis of Cylindrical OACS – all-Carbon 67
Figure 4.10: Modal Analysis of cantilevered cylindrical OACS – all - Glass and Hybrid 68

List of Tables

Table 2.1: Compressive strength of Yarn #6 at different span-lengths 18
Table 2.2: Cross-sectional area of yarn #6 23
Table 2.3: Statistical analysis on data set 26
Table 2.4: Pearson correlation coefficient 26
Table 2.5: Analysis of variance 27
Table 2.6: Parameter Estimates 28
Table 2.7: Predicted and residual values 30
Table 3.1: Stiffness test specimen 37
Table 3.2: OACS Tubes Stiffness comparison table 38
Table 3.3: Orthotropic material properties of carbon-fiber and glass-fiber 42
Table 3.4: Carbon OACS Modal results 46
Table 3.5: Glass OACS Modal Results 48
Table 3.6: Experimental Modal IROC-OACS Test specimen specification 49
Table 3.7: Exp. modal results initial IROC test specimen, carried out at NASA Glenn [6] 55
Table 4.1: First Modal frequency - Tapered OACS equal diameter yarns (IROC)12x6x6 60
Table 4.2: First Modal frequency - Tapered OACS (IROC)12x6x6 62
Table 4.3: Cylindrical IROC OACS Modal results for 16x8x8 69
Table 4.4: Cylindrical IROC OACS Modal results for 16x16x16 69
Table 4.5: Cylindrical IROC OACS Modal results for 24x12x12 69
Table 4.6: Cylindrical IROC OACS Modal results for Hybrid tubes 69
Table 4.7: Cylindrical IROC OACS Modal results for all carbon tube 70

List of Abbreviations

AU	Auburn University
CF	Carbon fiber
OACS	Open Architecture Composite Structures
CW	Clockwise
CCW	Counter clockwise
TT	True Triaxial
CT	Conventional Triaxial
FEA	Finite Element Analysis
FE	Finite Element
IROC	Integrated RF and Optical Communications (Satellite)
NASA	National Aeronautics and Space Administration
CTE	Coefficient of Thermal Expansion
RF	Radio Frequency

Chapter 1
Introduction

Carbon Fiber Composites

As Man tends to make use of energy more efficiently and to reach for greater heights to move beyond this Earth, he soon realizes that stronger, lighter, less expensive materials must be developed to achieve most of his goals.

Carbon fiber reinforced polymers (CRPF) is one of the most widely used lightweight, strong materials that we use today to achieve the above-mentioned characteristics.

CFRP is essentially a composite material comprised of carbon fibers and an epoxy resin matrix. The monofilament fibers are around 7 micro-meters in diameter and usually have either kidney or circular cross-section shapes. The material with the strongest fibers is polymer based and are often referred to as “whiskers” [1].

As the diameter of the fiber decreases to single-micron levels, single crystal structures have lower dislocation densities when compared to polycrystalline solids - this is the basis of strength aspect of a fibrous composite.

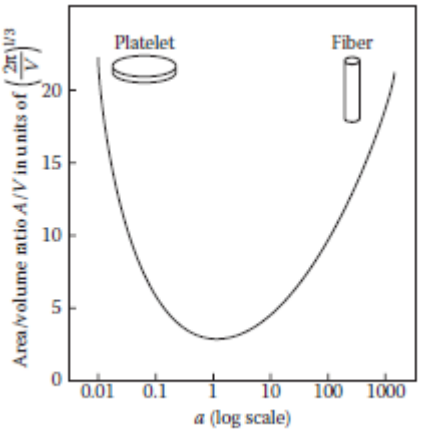

Figure 1.1: Surface area-to-volume ratio A/V of a cylindrical particle of given volume plotted vs. particle aspect ratio a = l/d

Figure 1.1 from Ref. [1], shows that the ratio of surface area to volume for a cylindrical particle is greatest when the cylindrical particle is either in fiber form or as a platelet. For the fibers, the aspect ratio (length-to-diameter ratio) given by, $a = l/d$ is very large and as for the platelet, the aspect ratio is very small. Thus, as the fiber length-to-diameter ratio increases, so does the fiber/matrix interfacial area available for stress transfer per unit volume of fiber increases.

Very high aspect ratio fibers allow us to obtain maximum tensile strength and stiffness of a material. However, they alone cannot be used to support longitudinal compressive loads, and the transverse mechanical properties are not as good as their longitudinal properties. Thus, fibers are held in a binder matrix material to provide strength and stiffness under compressive and transverse loading.

Composite Fabrication Using Carbon Fibers

Carbon fibers (CFs) are processed for specific applications in the industry by using different composite manufacturing processes. The type of fabrication process depends on factors such as design complexity, strength requirements and cycle time allocated for the manufacturing process. A few of the widely used composite manufacturing processes are Hand lay-up, spray-up, compression mold, filament winding and composite braiding processes.

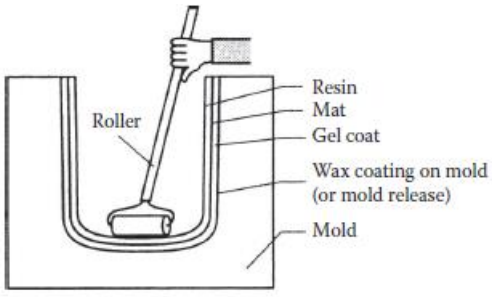

Figure 1.2: Hand lay-up composite fabrication

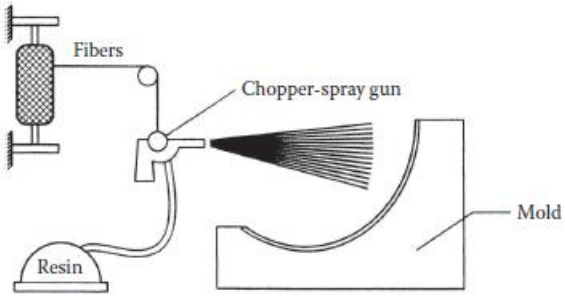

Figure 1.3: Spray-up composite fabrication

Two of the earliest and most widely used composite fabrication processes are the hand lay-up (Figure 1.2) and spray-up (Figure 1.3) processes. The process involves, a woven fiber fabric or

chopped strand mat in the case of hand lay-up and chopped fiber strands in case of spray-up process; these fiber forms are applied to the release treated mold followed by a thermoset resin. A roller is used to spread out the resin evenly across the contours of the mold and depending on the resin characteristics, it is either let to cure in the open or placed in an autoclave or a convection oven. Hand lay-up and spray-up processes are used for development of prototype parts or large production parts in small quantities.

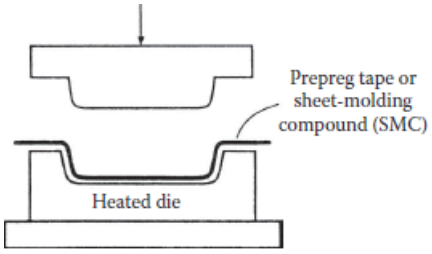

Figure 1.4: Compression molding

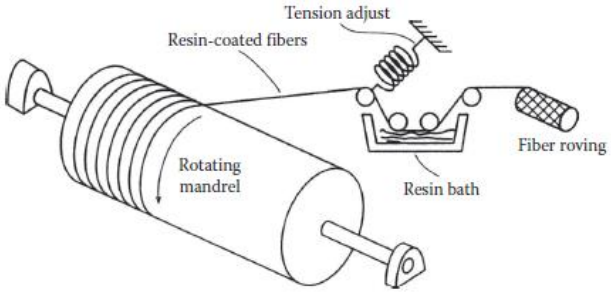

Figure 1.5: Filament winding process

The compression molding process Figure 1.4, generally uses prepreg tape which consists of fibers pre-coated with polymer resin. The prepreg tape is laid on the heated die and pressure is applied through the mold. Cure time for the composite depends on the polymer resin properties. High volume composite parts are manufactured using compression molding techniques.

Cylindrical composite components such as pressure vessels, rocket motor cases, power transmission shafts and, tubing are widely manufactured using the filament winding technique, Figure 1.5. Prepreg unidirectional fibers are placed on the rotating mandrel in a wrapping motion at a rate of one layer per revolution, and the mandrel is indexed after each revolution to offset the joints of prepreg tape by a small amount. Once the winding is completed, the mandrel is pressurized and cured in an autoclave to achieve maximum mechanical properties by reducing void content to as low as 0.1% [1].

This work focusses on the “composite braiding processes,” which works on the Maypole braiding principle. The process is explained in-detail in the following sections.

Composite Braiding Manufacturing Process

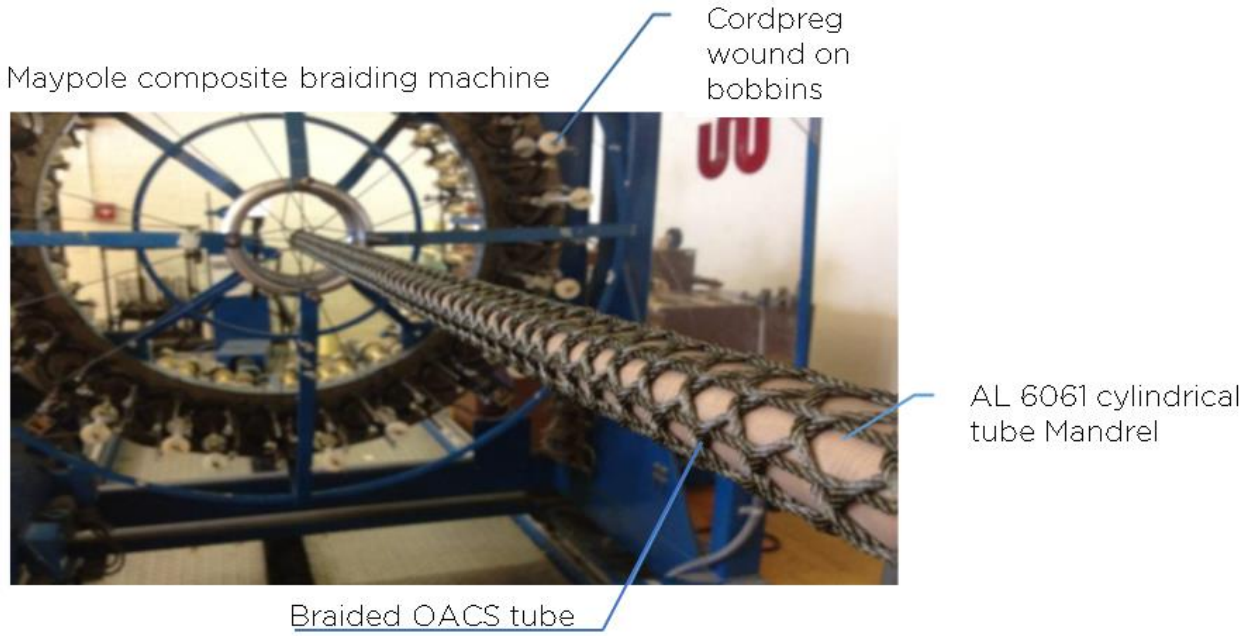

Figure 1.6: OACS Braiding Process

This work explores ways to improve the compressive strength of the Open Architecture Composite Structures (OACS) tubes of uniform cross section. The OACS are braided on a composite braiding machine and the structures take the shape of the mandrel they are braided on.

The process of braiding composite structures allows the creation of open lattice structure which is light weight and extremely stiff and at the same time uses concepts developed from structural optimization by using geometry to minimize the mass of the structures without compromising the strength characteristics. The best example for geometric optimizations can be found in trusses used in structural design. The maypole braiding process enables braiding composite structures to provide efficient load transfer throughout the truss geometry. Branscomb et al [3] and Gurley et al [4] covers the design, development and optimization of the OACS tubes.

Braiding Process Flow

Figure 1.7: OACS Manufacturing Process Flow

Tow Preg

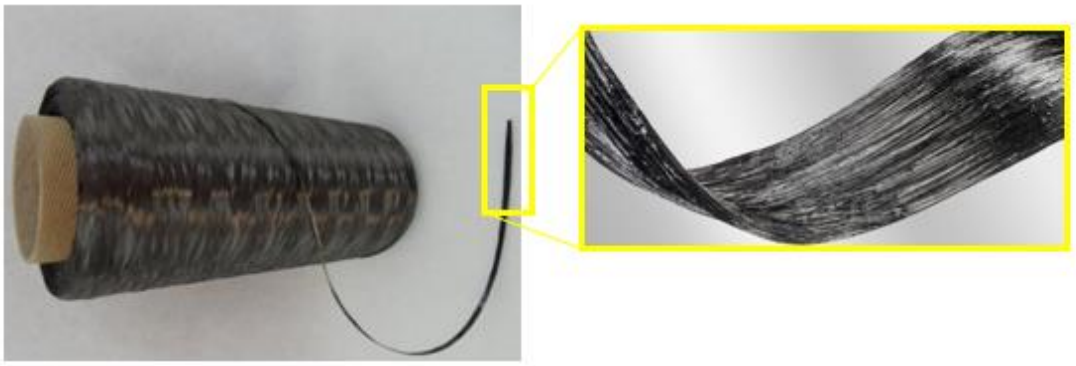

Figure 1.8: Carbon Fiber Tow, Toray T700s

Carbon fiber tows come as spools of carbon fiber filaments and are available in sets of multiples of 1000 filament tows. The tow spools are referred to as 3K, 12K, and 48K and contain 3000 fibers, 12000 fibers and 48000 fibers respectively. Tow pregs in their raw form are often used in the filament winding processes, carbon fiber fabric weaving processes, and unidirectional pultrusion processes.

Braiding Tow Pregs Into Yarns

Figure 1.9: Braided tow preg (yarn)

In this work, prepreg carbon tows of 48K and 72K, as core material have been used to braid the yarns. The braid weave pattern in the jacket of the yarn#6 is a true triaxial braid [12] [8] with Nylon, Vectran and Carbon tows. The process of braiding the tow preg into a yarn forms the tow pregs into a cylindrical shape which increases the area moment of inertia after the cure process. This helps in improving the overall stiffness of the structures that utilize the yarns.

Without the braided yarns, it would be very difficult to braid composite structures on conventional braiding machines and hence it is a critical step in the OACS manufacturing process.

Braiding OACS Tubes

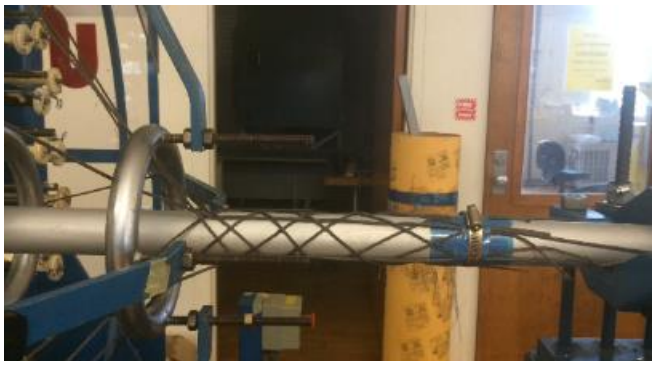

Figure 1.10: Braiding OACS tubes

The OACS tubes were manufactured on a composite braider machine which operates on the Maypole braiding principle. Based on the geometry of the required structure a braiding machine with 32,64 carriers strategically loaded with yarn bobbins have been be used to manufacture the

tubes. The diameter of the mandrel determines the diameter of the OACS tube. The traverse velocity, angular velocity and loading of the carrier bobbins all result in a kind of braided OACS tube and must be carefully considered before the manufacturing stage.

Once the braiding is complete, the braided structure along with the mandrel was cured in a large convection oven, the cure temperature and cure time are dependent on the type of prepreg epoxy resin. The tows used in this work are Toray T700s for the core and T300 for the axials in the jacket with UF3330 prepreg epoxy resin, cure temperature of 125^{o} C and cure time of 4 hours [10].

Chapter 2
Braided Yarn Compression Testing and Failure Modes

Introduction and Scope of Work

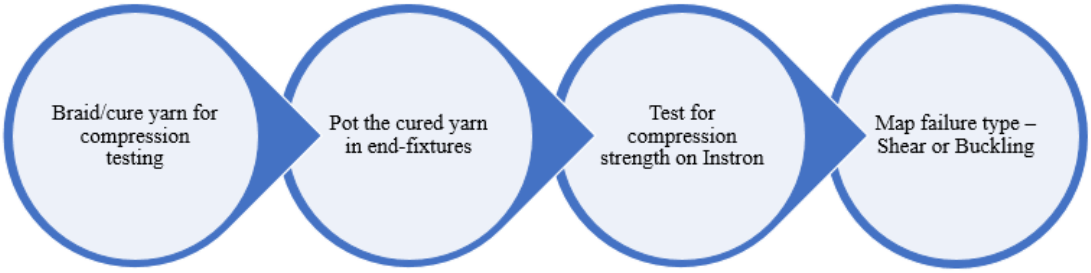

Figure 2.1: Yarn Compression testing flow chart

Experimental testing carried out by Kothari [7] and Shirgaonkar [9] on the OACS tubes and braided yarns covers tensile testing, 3-point bend test, test for flexural modulus and other mechanical properties. During the time of this work, compression tests on braided yarns had not been carried out and this chapter involves details about the manufacturing of yarn#6. Design and development of the experimental testing procedure used to find the compressive strengths of yarn number 6 has also been covered in this chapter.

Figure 2.1 illustrates the process flow involved in testing the yarns for compression strength and the details are explained in the following sections.

Braiding and Curing of Cordpreg for Compression Test

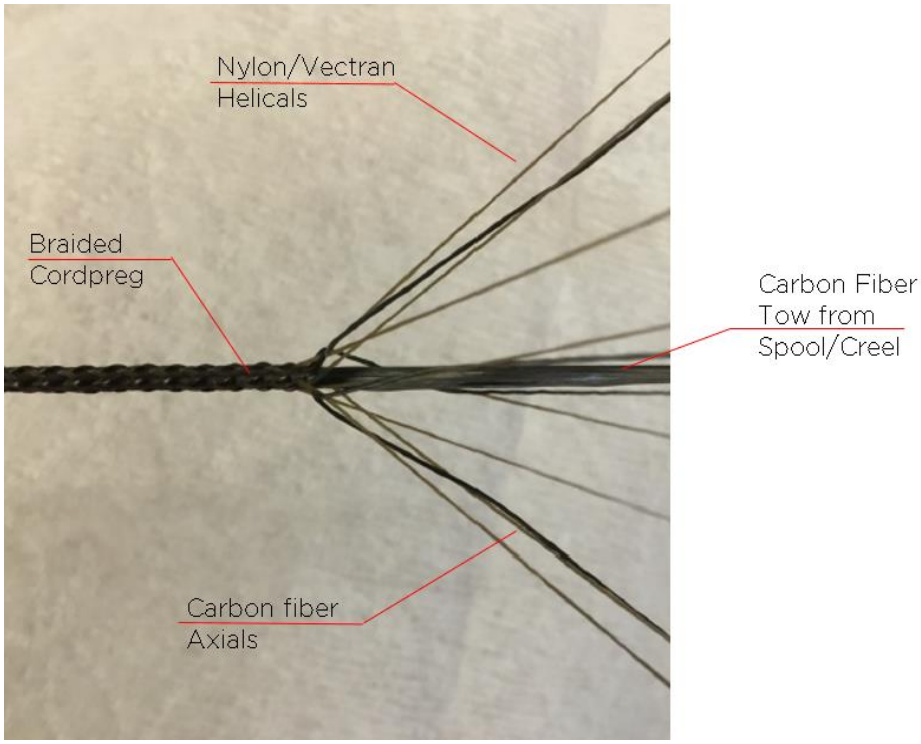

Figure 2.2: Braiding of Yarn #6; Photograph from [2]

Figure 2.2 shows the braiding of yarn #6. The yarn was braided on a 32-carrier composite braiding machine. Yarn construction (identified as yarn number 6) was selected for the purposes of this work. The construction of the cord preg consists of 48K T700s carbon fiber tows, and the braided jacket around the core is of a true triaxial architecture [8] [12] with 8 number of 500 Denier textured Nylon helical yarns in clockwise and counter clockwise directions and 4 number of 3K T300 prepreg carbon axials. Once the yarn is cured, the outside diameter of yarn #6 is around 2.38 mm.

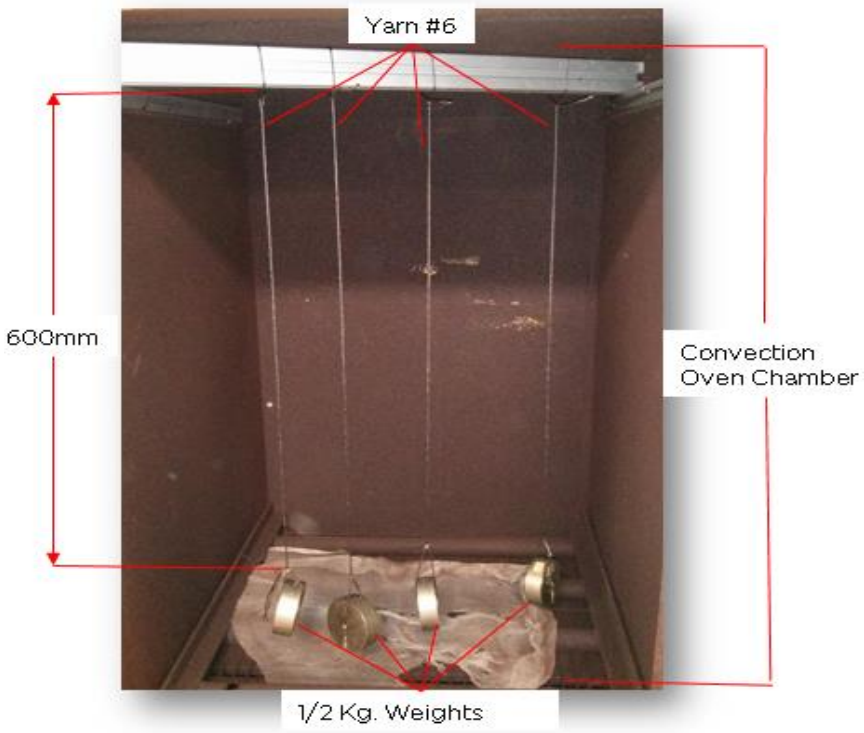

Figure 2.3: Yarn #6 - Oven Curing

After the braiding process, Yarn #6 was cut into 600 mm lengths, and was tied down with 0.5 Kg. weights to induce tension and maintain straightness. The samples were then placed in a convection oven as shown in Figure 2.3. The cordpreg yarn with pre-impregnated T700s carbon fiber core and UF3330 epoxy resin was cured at 125º C for 4 hours [10]. To avoid thermal-shock the cured yarns were let to cool down to room temperature before removing them from the oven. The cured yarns were cut to the proper compression test specimen lengths in preparation for the compression test.

Design and Development of Yarn - Compression Test Fixtures and Specimen

To test the compression strength of different span-lengths of braided yarn #6, spherical groove, cylindrical flat-end hole, cap-nut end, hex groove yarn compression test fixtures were designed and machined. The development and results from each type of design is explained in-detail below.

Spherical Compression Test Fixture

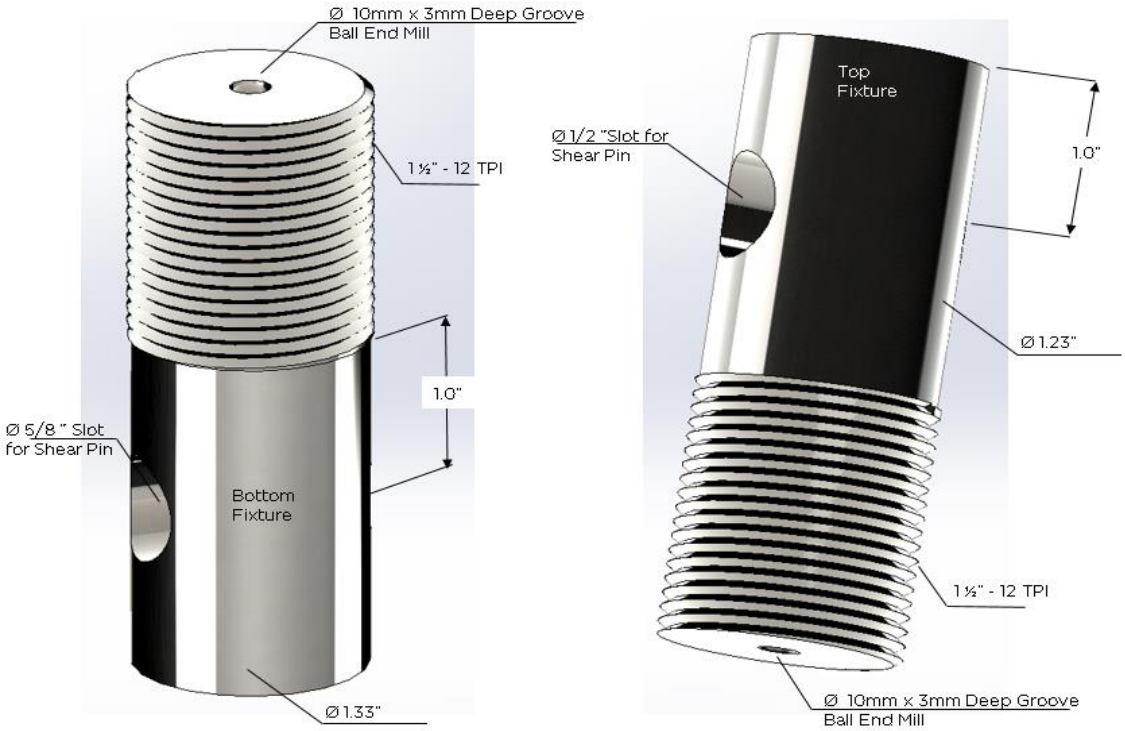

Figure 2.4: Spherical Groove Compression Test Fixture

The compression tests were carried out using an Instron 5500 material testing system. Special compression fixtures had to be designed and machined for testing the cordpreg yarns and had to be compatible with the Instron 5500 attachments.

Figure 2.4 illustrates the spherical groove compression fixture. The bottom fixture mounts to the movable cross head on the Instron 5500 and the top fixture mounts to the fixed cross head. Both the fixtures are constrained to the Instron attachments via the shear pins and 1 ½ "– 12 TPI nut. A spherical groove 3 mm deep was milled on the face of the fixtures with a 10 mm ball nose end mill. The grooves serve the purpose of aligning the spherical end compression test specimen during the compression test. The fixture design remains the same with slight modifications to accommodate cylindrical flat-end hole, cap-nut and hex nut compression test specimens.

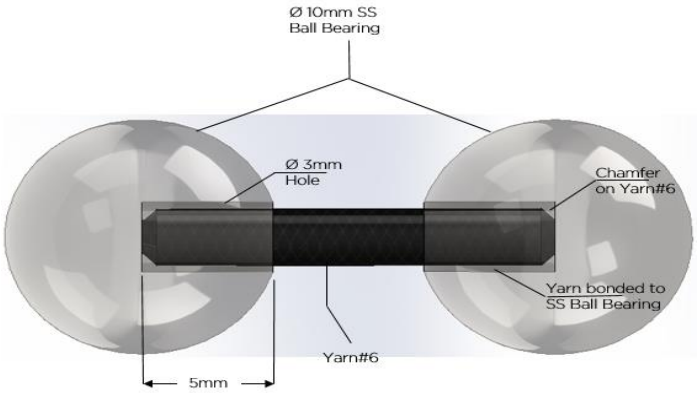

Figure 2.5: Spherical End Compression Test Specimen

As shown in Figure 2.5, holes of 3 mm diameter and 5 mm deep were drilled in stainless steel ball bearings of 10 mm diameter. The yarn #6 braided compression test samples were bonded to the stainless steel ball bearings with DP460 epoxy adhesive and cured for 24 hours at room temperature. Yarn specimen samples were made to accommodate 5 mm potted depth at each end and had a chamfer for easier assembly.

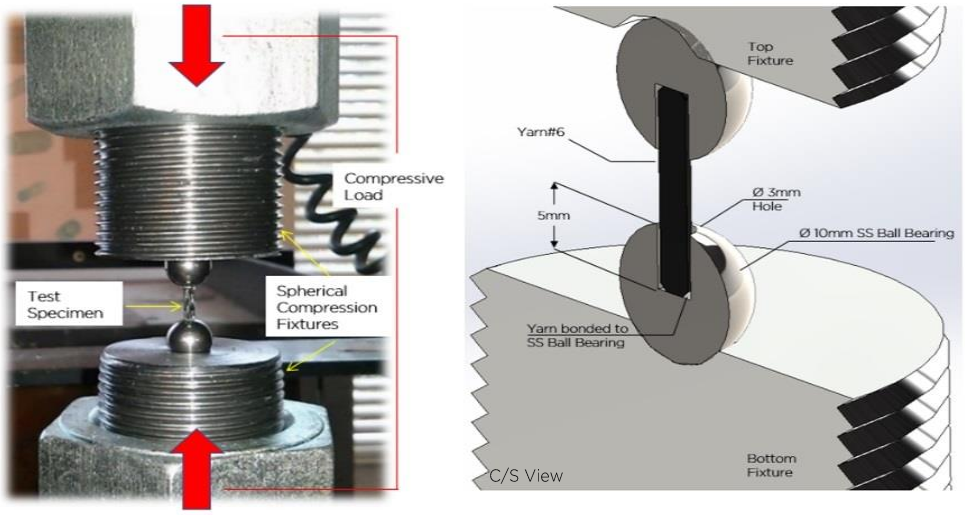

Figure 2.6: Spherical-end compression test method

The Compression tests carried out by the spherical ball method yielded one of the best compressive strength values as compared all other types of end-connections. Drilling precision holes in the ball bearings and careful assembly of test specimens were a limiting factor in using them as the standard test method in this work.

Cylindrical Flat-End Hole Compression Test Fixture

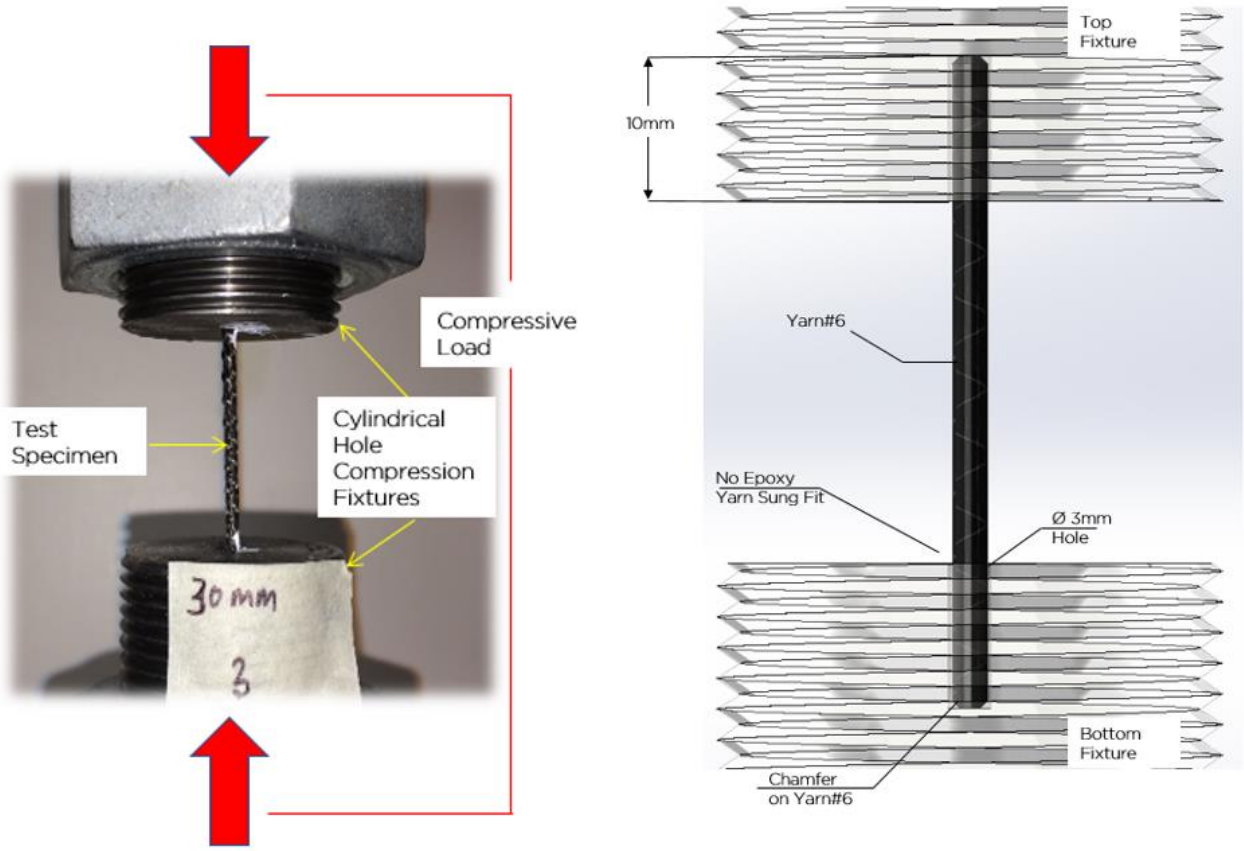

Figure 2.7: Cylindrical Flat-End hole compression test method

To replicate the fixed-fixed boundary condition for compression testing of the yarn, 3 mm holes were drilled on the top and bottom compression fixtures, the holes were slightly larger than the diameter of the yarn. To position the yarn specimen in the holes, the edges of the test specimen were chamfered. The specimens were *not* potted with epoxy and the fit relied on the close tolerance between the yarn and the hole diameters. Yarn specimens were compressed till the breaking load. Results indicated crushing of the yarns at the supported ends and the experiment did not yield accurate compressive strength values.

Cap-Nut End Compression Test Fixture

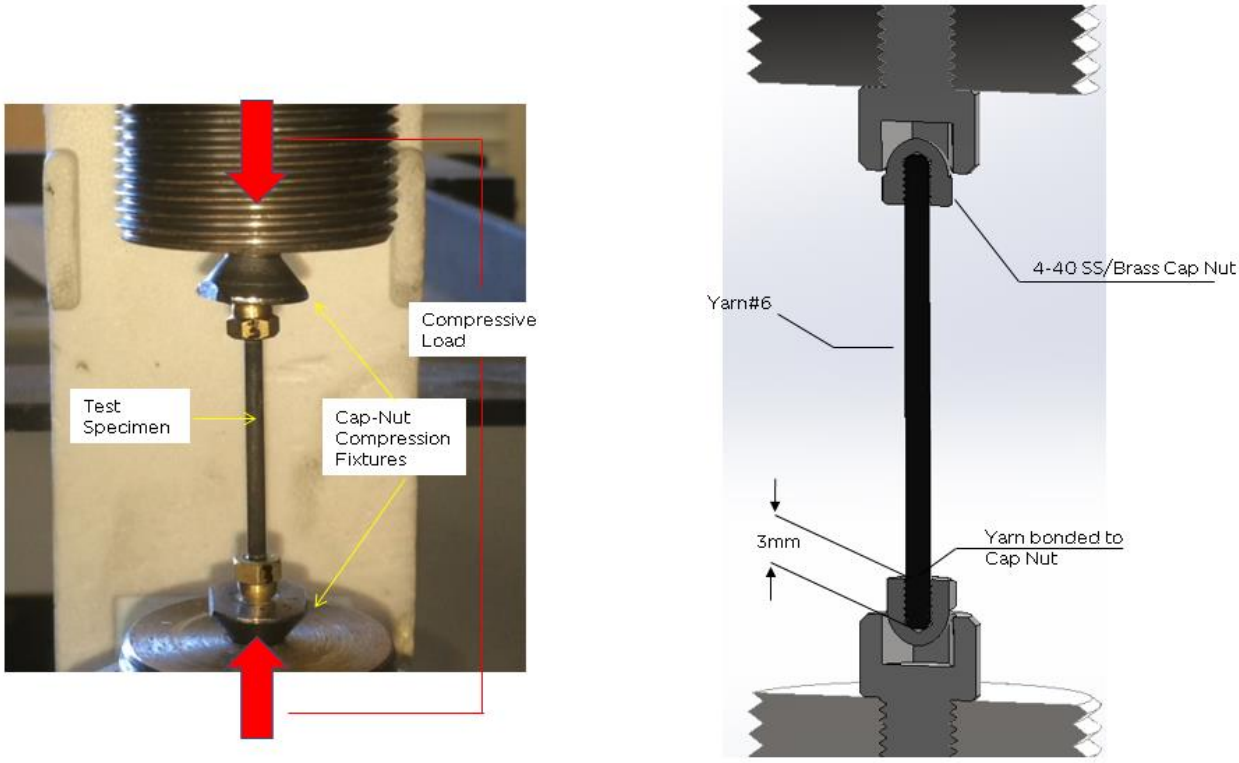

Figure 2.8: Cap-Nut compression test method

Braided yarns with cap-nut ends were tested as an alternative to the spherical ball ends; these were similar to the spherical ball, and had precision holes drilled for potting the yarn. Figure 2.8 shows two 4-40 cap nuts with yarn #6 potted with DP460 epoxy adhesive. The potting depth of 3 mm available in the cap nut was insufficient for the compressive loads the samples were subjected to, and the braided yarn would slip within the end connections.

Hex-End Compression Test Fixture

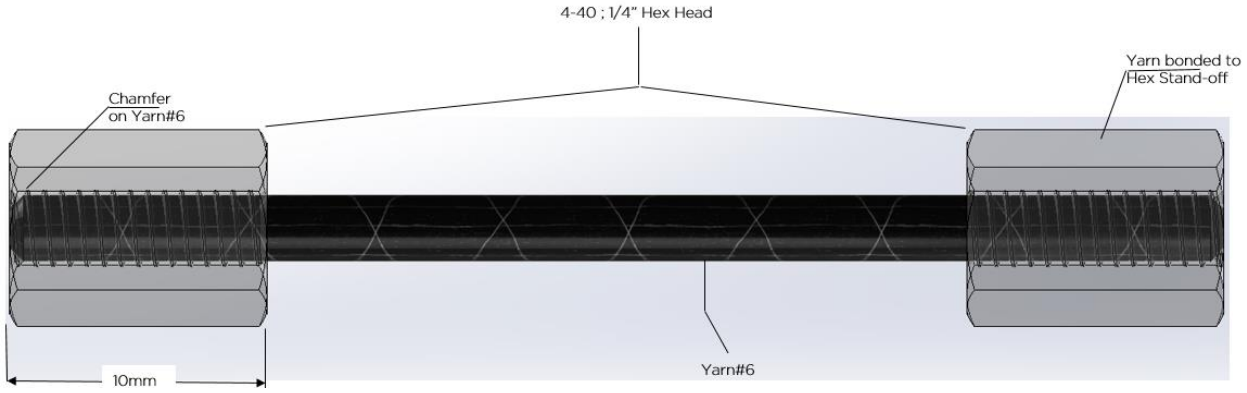

Figure 2.9: Hex End compression test specimen

The hex-end yarn #6 compression test specimen uses two 4-40 stainless steel hex stand offs. The yarn was potted between the stand offs with DP460 epoxy adhesive and cured at room temperature for 24 hours. As illustrated in Figure 2.9, the distance between the hex stand offs is the span-length of the test specimen and the potting depth is 10 mm at each end. The yarn samples had chamfered edges for easier assembly.

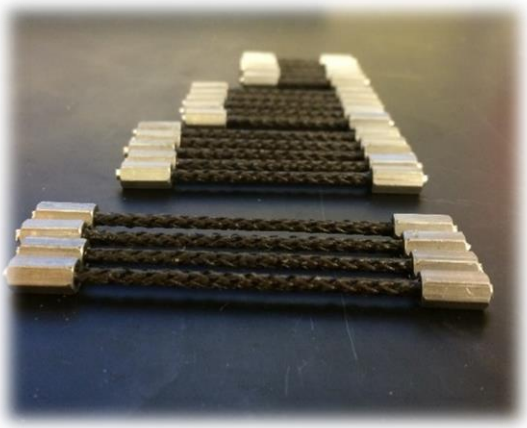

Figure 2.10: Hex End Yarn #6 compression test specimens

Figure 2.10 shows hex-end compression test samples of increasing span-lengths ready for compression test.

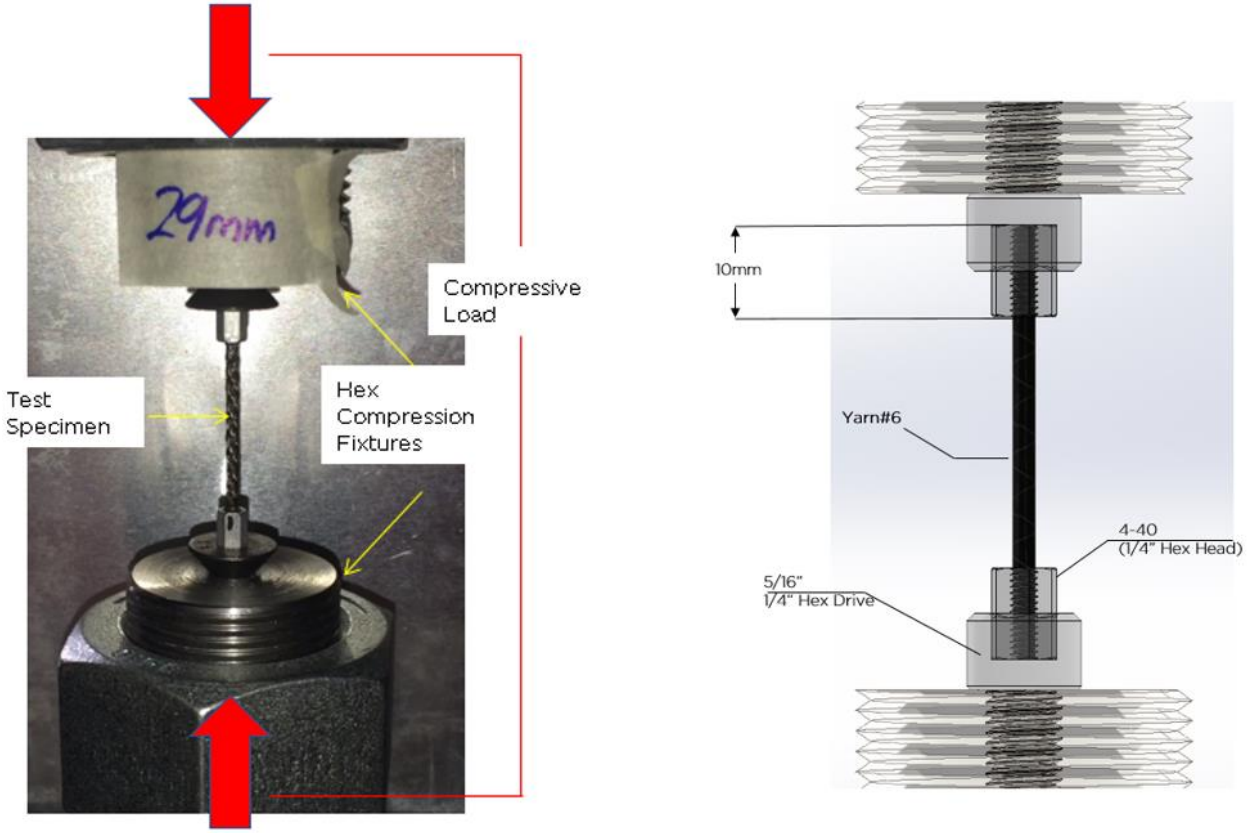

Figure 2.11: Hex-end compression test method

Hex standoff nuts provided a fixed-fixed boundary condition, wherein, the potted yarn samples were positioned in a hexagonal socket head screw (5/16 -24 ¼" hex drive) in the compression fixture.These fixtures had the right amount of potting depth to accommodate the yarns and were simple to make multiple test samples in a short amount of time.

The compression strength results obtained this condition were similar to the spherical ball ends, and no slippage or debonding of the test samples were observed.

The compression strength of yarns in this research work has all been carried out using hex stand-off nuts as the potted ends.

Compression Loading of Yarn #6 at Different Span-lengths

Previous work on yarn #6 was carried out to find the tensile properties [7]. This work focusses on finding the compressive loads that the yarn can handle and to find the buckling/lateral bending loads of yarn #6. Multiple span-lengths of the yarn ranging from 7 mm all the way up to 100 mm were tested.

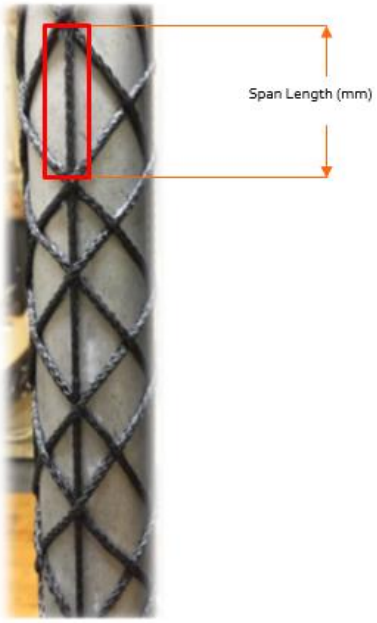

Figure 2.12: Axial yarn Span-length in OACS

The specifications of yarn #6 is as follows,

Core carbon fiber count: 48K

Carbon fiber in Jacket: 4*x*3K Tow pregs

Nylon Yarn in Jacket: 8*x*500 Denier Helical

Braid: True Triaxial

The span-lengths were chosen based on the longest axial yarns that support the OACS during compressive loading. Experimental testing showed the axial yarns were to either buckle or exhibit brittle-fracture under compressive loads [9] [2] and to better understand the failure modes and improve the OACS design, experimental testing on different spans of yarn #6 were carried out.

Table 2.1: Compressive strength of Yarn #6 at different span-lengths

Sample Length (mm.)	Sample No.	Compressive Load (N)	Mean Load (N)
7	1	2596.61	2542.11
	2	2548.32	
	3	2711.76	
	4	2311.22	
8	1	1624.64	1983.67
	2	2441.14	
	3	1570.42	
	4	2298.61	
12	1	1063.71	1186.2
	2	1624.75	
	3	959.34	
	4	1097.22	
15	1	1030.26	1091.6
	2	1060.98	
	3	1065.92	
	4	1146.83	
18	1	1323.61	1334.1
	3	1460.94	
	4	1217.89	
24	1	1251.66	1021.6
	2	828.42	
28	1	1176.11	1366.91
	2	1258.67	
	3	1470.53	
	4	1435.44	
32	1	1220.31	1174.22
	2	1280.42	
	3	1162.47	
	4	1079.72	
39	1	763.32	822.91
	2	964.23	
	3	733.97	
	4	776.37	
49	1	618.28	698.56
	2	780.12	
	3	702.14	
	4	693.69	
60	1	464.21	454.811
	2	432.2	
	3	468.01	
72	1	243.88	256.84
	2	236.11	
	3	290.55	
	4	110.56	
82	1	105.57	117.64
	2	136.78	
	3	335.72	
90	1	282.07	287.43
	2	244.51	

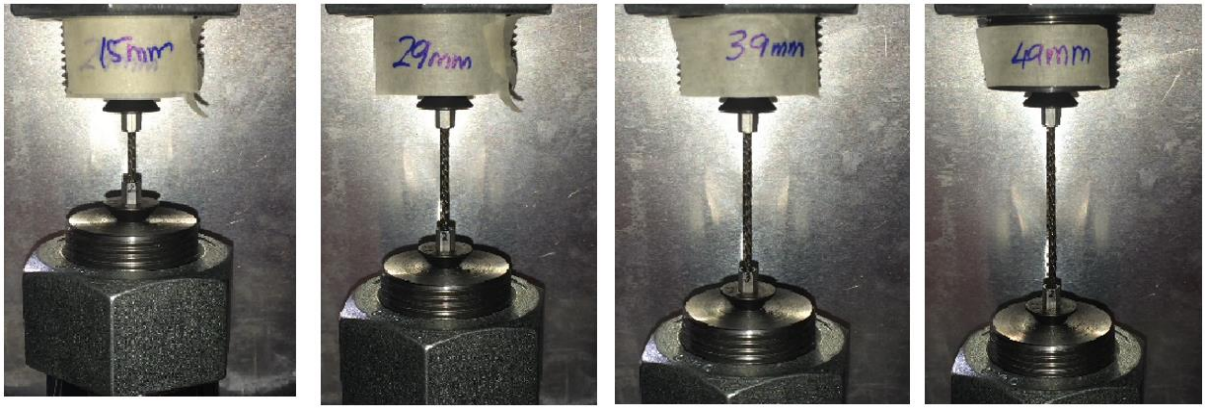

Figure 2.13: Compression test specimen – yarn #6

Figure 2.13 shows the fixed-fixed end condition (hex-end) yarn #6 compression test samples of varying lengths.

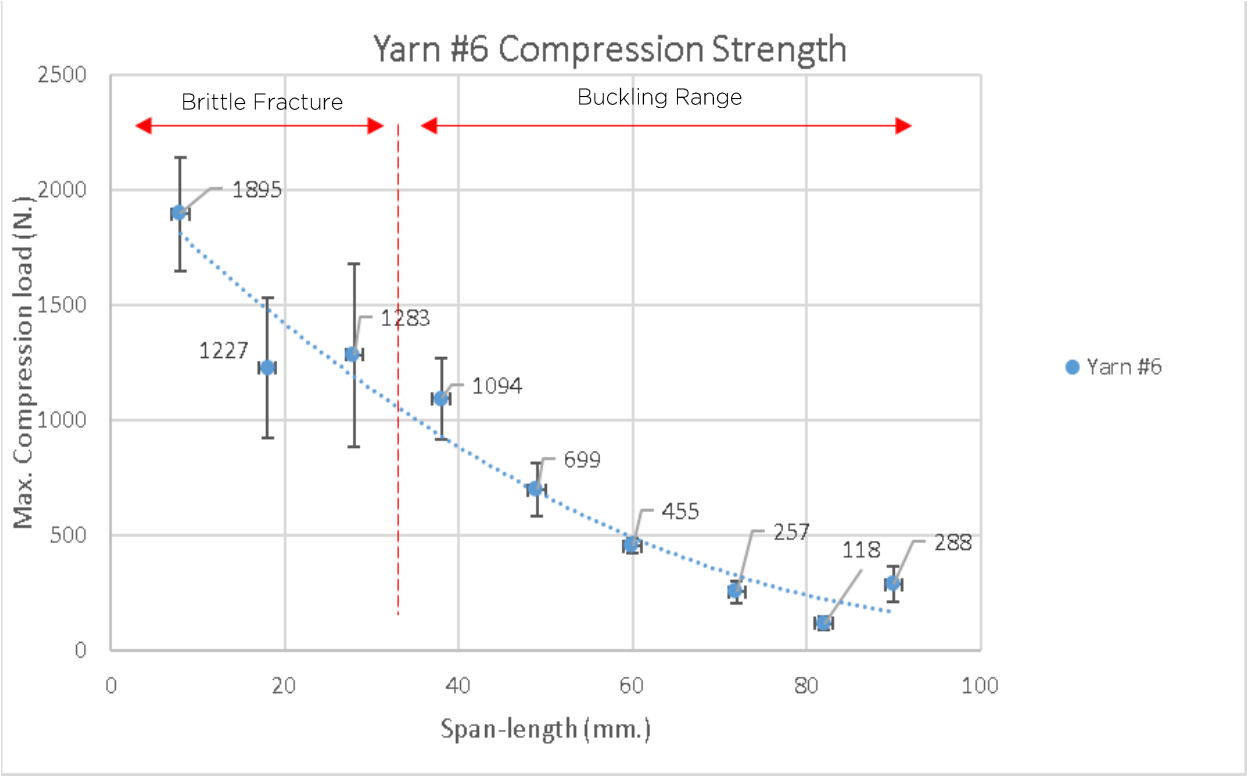

Figure 2.14: Compression loading of braided yarn #6

Figure 2.14 represents the data set of maximum compression loads of yarn #6 at various span-lengths. As explained previously, the lengths were based on the span-length of the axial yarns found on the OACS tubes. The dataset in Figure 2.14 has a trendline with polynomial fit. Yarn #6 test specimens were prepared for lengths in the range of 7 mm to 90 mm and were subjected to compressive loading, with the intention of capturing the failure loads of the yarn; the type of failure and the span-length of the failed yarn would help to improve the design of the OACS tubes by controlling the braid parameters to either match or avoid certain yarn span-lengths depending on the situation.

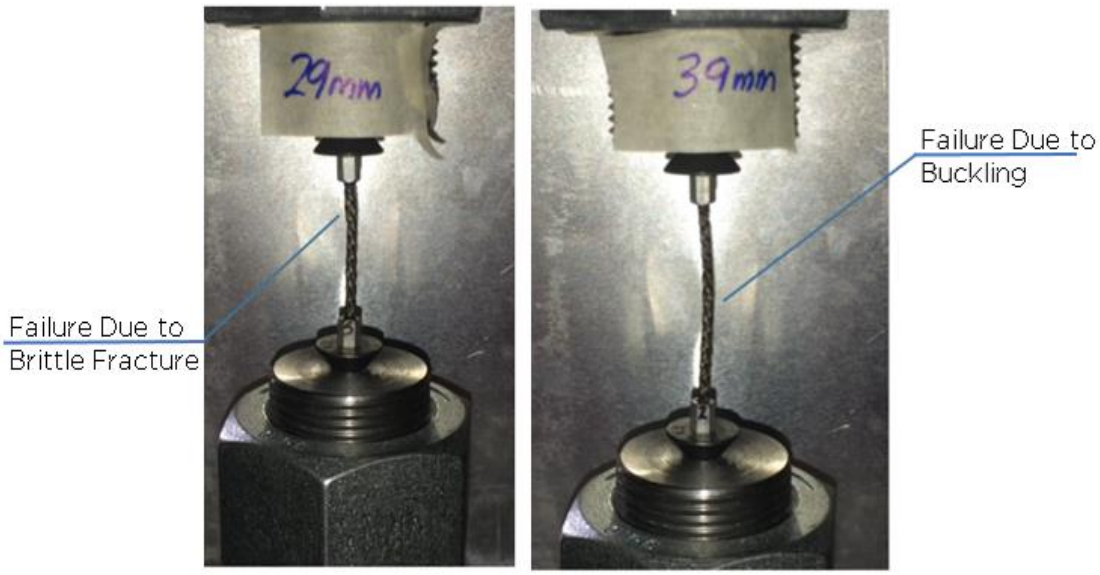

Figure 2.15: Brittle-fracture and Buckling failure

During experimental testing, it was observed that, Yarn #6 showed signs of buckling in the range of greater than 35 mm span-length as illustrated in Figure 2.15., the yarn sample of span-length 39 mm shows clear signs of bending off-axis before failure and the yarn with span-length 29 mm experiencing a brittle fracture with failure along the estimated 45^{o} plane.

Yarn #6 Comparisons

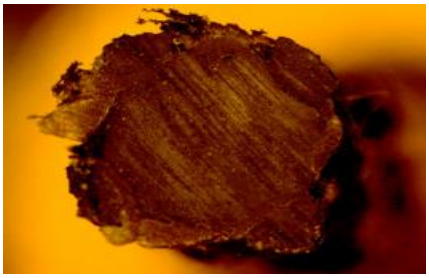

Figure 2.16: C/S of yarn #6 with jacket

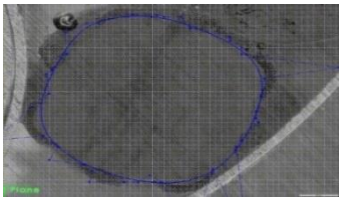

Area	Mean	Min	Max
3.217	35.391	0	255

Figure 2.17: C/S area of yarn #6 core w/o jacket

Assuming a perfectly square cross section of yarn #6 [2], the cross-sectional area, A_{Jacket} measured was 5.29 mm^2; the cross-sectional area, A of the core without jacket for yarn #6 obtained by observations under an optical microscope was 3.217 mm^2.

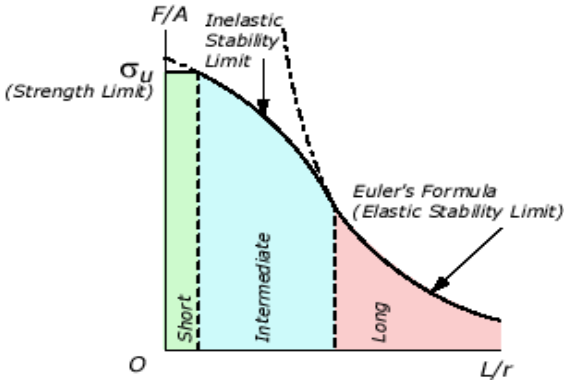

Figure 2.18: Euler Curve [5]

Euler critical load is given by,

$$P_{cr} = \frac{\pi^2 EI}{(KL)^2} \quad (1)$$

P_{cr} = critical or maximum axial load on the column just before it begins to buckle

E = (EI/I) = flexural modulus; 41.51 GPa, [7]

I = least moment of inertia for the column's cross-sectional area

L = unsupported length of column

For design purposes, the above equation can be written in terms of critical stress, by using $I = Ar^2$, where A is the cross-sectional area and r is the radius of gyration of the cross-sectional area. We have,

$$\sigma_{cr} = \frac{\pi^2 E}{(L/r^2)} \tag{2}$$

$$r = \sqrt{I/A} \tag{3}$$

σ_{cr} = critical stress, which is an average normal stress in the column just before the column buckles. It is required that $\sigma_{cr} \leq \sigma_Y$.

r = smallest radius of gyration of the column

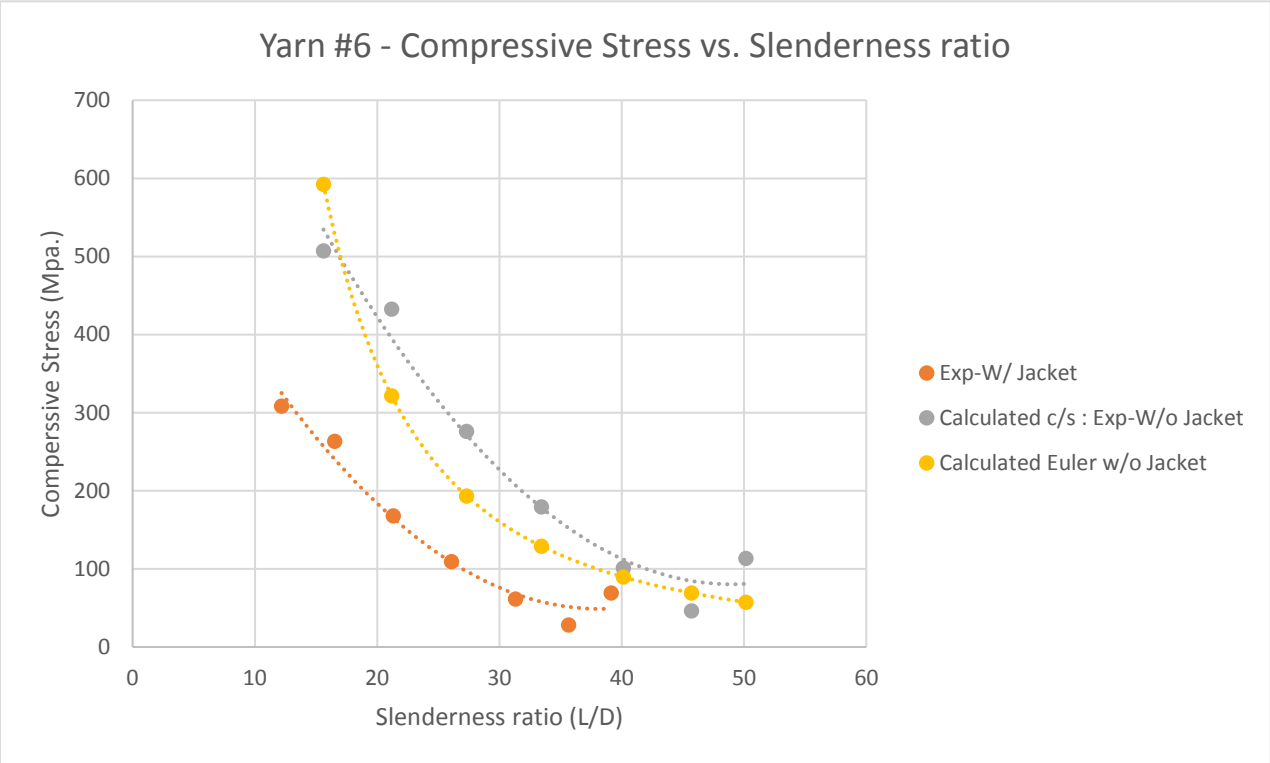

Figure 2.19: Yarn #6 - compressive stress vs. slenderness ratio

Table 2.2: Cross-sectional area of yarn #6

Yarn #6	Cross-sectional Area in mm^2
Experimental with Jacket	5.29
Experimental without Jacket (Calculated)	3.217
Euler without Jacket	2.52

Table 2.2 illustrates the cross-sectional area used in calculating the radius of gyration and the critical compressive stress of yarn #6 considering the effect of "with jacket" and "without jacket". The core at the center of the yarn makes up for most of its strength during compressive loading and by considering just the core cross-sectional area, the slenderness ratio is around 18 to 20. The slenderness ratio is significantly higher compared to the previous range of 12 to 16, having considered the jacket of the yarn to play a significant role in taking up compressive loads.

Conclusions from Compression Testing of Yarn#6

During the time of this work, yarn #6 was the most effective yarn braided at Auburn University and the development has been well documented based on work done by Austin Gurley [4], Nakul Kothari [7] and David Branscomb [3]. The range of span-lengths between 7 mm and 20 mm tested were found to have the highest compression strengths and the failure type observed for the yarns with span-lengths up to 35 mm was mostly brittle-fracture failure and little or no buckling/lateral bending phenomenon was observed in these ranges.

Yarn #6 with span-lengths over 35 mm and up to 100 mm showed significant signs of lateral bending/buckling like characteristics and had significantly lower compressive load bearing ability. Compression testing of yarns to find buckling modes was challenging due to the requirements in close tolerance of the fixtures to perfectly maintain the alignment of the yarn test specimen along the loading axis.

Spherical ball end fixtures proved to be the best way to test the yarns since, slight misalignments of the yarn along the loading axis would be countered by the spherical ends in the fixture. Future work on compression testing of yarns should be carried out with spherical end fixtures with a sample size of at least 30 number of yarns per span length.

Compression Breaking Load Prediction of Carbon Fiber Braided Yarn #6 Using Statistical Linear Regression Analysis

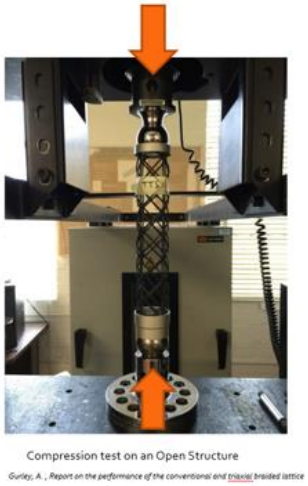

Compression test on an Open Structure

Gurley, A. , Report on the performance of the conventional and triaxial braided lattice

Testing the overall structure for compressive strength

Span Length (mm)

Trade off…

- *Shorter* the Span Length, *higher* the load carrying capacity
- *Longer* the Span Length, *lower* the mass of the entire structure, *higher* the chances for buckling

Figure 2.20: Yarn span-length

Research Considerations

Slight variation in the span-length of the OACS tube has a direct impact on its load carrying capacity, the mass of the entire structure and hence, the design of the OACS tube. It is necessary to test different span-lengths to check for the corresponding maximum compressive loads. However, it is *not* practical to test for every single millimeter change and hence, a simple linear regression analysis was performed to interpolate for the missing sample lengths and predict the corresponding compression loads.

Simple Linear Regression

Linear regression fits a data that is linear in the model coefficients. The most common type of linear regression is a least-squares fit, which can fit both lines and polynomials, among other linear models, [17].

Linear regression models the relation between a dependent, or response, variable *y* and one or more independent, or predictor, variables $x_1 \ldots x_n$. Simple linear regression considers only one independent variable using the relation, $y = \beta_o + \beta_1 x + \varepsilon$; where, β_o is the *y*-intercept, β_1 is the slope (or regression coefficient), and ε is the error term, [17].

Experimental Observations

```
data dl;
input Observation x y;
label y='Load (N)' x='Span Length (mm)';
cards;
```

1	32	916.941
2	32	1280.47
3	32	1162.47
4	32	873.7
5	32	1079.72
6	38	1153.67
7	38	1026.41
8	38	981
9	38	1077.83
10	38	1230.65
11	49	618.285
12	49	780.148
13	49	702.141
14	49	693.7
15	60	464.211
16	60	432.209
17	60	468.013
18	72	243.88
19	72	236.112
20	72	290.552
21	82	110.565
22	82	105.572
23	82	136.785

Span lengths
1. 32mm
2. 38mm
3. 49mm
4. 60mm
5. 72mm
6. 82mm

Testing a cured yarn for compressive strength (this depicts the span length in the structure)

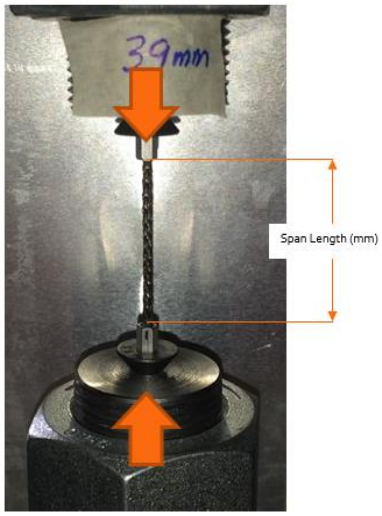

Figure 2.21: Experimental data

Compression test data for samples ranging from 32 mm to 82 mm were considered for the Simple linear regression statistical analysis to provide estimates of compression loads for different span-lengths within the range of the experimental data set [14]. The least squares

regression model is used to explore how change in span-length affects the maximum compression load and allows us to predict the value of one variable given the value of the other. Simple linear regression should only be used to predict the load values inside the range of the experimentally tested values of span-length without extrapolating the values [14].

Hypothesis and Testing for Correlation:

Null Hypothesis $H_{0,}$ ρ (correlation) is equal to zero; Alternate Hypothesis H_A**,** ρ (correlation) is not equal to zero

Table 2.3: Statistical analysis on data set

Simple Statistics							
Variable	N	Mean	Std Dev	Sum	Minimum	Maximum	Label
x	24	51.12500	17.76492	1227	32.00000	82.00000	Span Length (mm)
y	23	698.47974	392.60235	16065	105.57200	1280	Load (N)

Table 2.4: Pearson correlation coefficient

Pearson Correlation Coefficients Prob > |r| under Ho: Rho=0 Number of Observations		
	x	y
x Span Length (mm)	1.00000 24	-0.95812 <.0001 23
y Load (N)	-0.95812 <.0001 23	1.00000 23

Table 2.4 includes information on the Pearson correlation coefficient, it is a measure of the linear correlation between the variable *X* (Span-length) and the variable *Y* (Maximum Compressive Load), the value of -0.95812 represents a strong negative relationship between the increase in span-length and the compressive load carrying ability of the braided yarn.

Variables of Interest

Dependent Variable: Maximum Compression Load (N); Independent Variable: Span-length (mm)

Hypothesis for Regression

Null Hypothesis H_0**:** β_1(Slope of Regression Line in population) equal to zero.

Alternate Hypothesis H_A**:** β_1(Slope of Regression Line in population) not equal to zero.

Model Parameters

Table 2.5: Analysis of variance

Source	DF	Sum of Squares	Mean Square	F Value	Pr > F
Model	1	3112908	3112908	235.07	<.0001
Error	21	278097	13243		
Corrected Total	22	3391005			

$$\frac{SSM}{SST} = r^2 \quad ; \quad r^2 = \frac{3112908}{3391005} = 0.918 \tag{4}$$

$$t = \sqrt{F} \quad ; \quad t = \sqrt{235.07} = 15.33 \tag{5}$$

Table 2.5 includes information concerning model fit. The *F* statistic for the overall model is highly significant ($F = 235.07$, $p<0.0001$), indicating that the model explains a significant portion of the variation in the data. The degrees of freedom can be used in checking accuracy of the data and model. The model degrees of freedom are one less than the number of parameters to be estimated. This model estimates two parameters, β_o and β_1; thus, the degrees of freedom should be *2 - 1 = 1*. The corrected total degrees of freedom are always one less than the total number of observations in the data set, in this case *23 – 1 = 22.* [18].

The square of the correlation (r^2 = *r-square*) is the proportion of the variance in the values of *y* that is explained by the least squares regression of *y* on *x*. r^2 *=0 .918* means 91.8% of the variance in compression load is explained by the least squares regression line on span-length.

Table 2.6: Parameter Estimates

Variable	Label	DF	Parameter Estimate	Standard Error	t Value	Pr > |t|
Intercept	Intercept	1	1779.62255	74.48692	23.89	<.0001
x	Span-length (mm)	1	-20.93122	1.36521	-15.33	<.0001

The "Parameter Estimates" Table 2.6 contains the estimates of β_0 and β_1. The table also contains the *t* statistics and the corresponding *p*-values for testing whether each parameter is significantly different from zero. The *p*-values (t = 23.89, p = <0.0001 and t = -15.33, p = <0.0001) indicate that the intercept and span-length parameter estimates, respectively, are highly significant. From the parameter estimates, the resulting model is,

Compression Load = 1779.622 - 20.931*Span-length

SAS Code for Simple Linear Regression

```
data d1;
input Observation x y;
label y='Load (N)' x='Span-length (mm)';
cards;

1       32      916.941
2       32      1280.47
3       32      1162.47
4       32      873.7
5       32      1079.72
6       38      1153.67
7       38      1026.41
8       38      981
9       38      1077.83
10      38      1230.65
11      49      618.285
12      49      780.148
13      49      702.141
14      49      693.7
15      60      464.211
16      60      432.209
17      60      468.013
18      72      243.88
19      72      236.112
20      72      290.552
21      82      110.565
22      82      105.572
23      82      136.785
24      39      .
;
run;
ods rtf
file="\\spirit.auburn.edu\SZM0082\Downloads\Project\Buck
ling_xy.rtf";
 proc corr data=d1;
 var x y;
 run;
proc reg data=d1;
  title1 height=12pt 'Scatterplot of Load by Length with
regression line (proc reg)';
  model y = x / cli clm;
  ods exclude nobs FitStatistics;
run;
quit;
ods rtf close;
```

Define *x* and *y* variables

Input data set

Run simple linear regression analysis, output fit and residual plots

Table 2.7: Predicted and residual values

The REG Procedure
Model: MODEL1
Dependent Variable: y Load (N)

Output Statistics						
Obs	Dependent Variable	Predicted Value	Std Error Mean Predict	95% CL Predict		Residual
1	917	1110	35.9943	859.0743	1361	-192.8826
2	1280	1110	35.9943	859.0743	1361	170.6464
3	1162	1110	35.9943	859.0743	1361	52.6464
4	874	1110	35.9943	859.0743	1361	-236.1236
5	1080	1110	35.9943	859.0743	1361	-30.1036
6	1154	984.2363	30.3834	736.7196	1232	169.4337
7	1026	984.2363	30.3834	736.7196	1232	42.1737
8	981	984.2363	30.3834	736.7196	1232	-3.2363
9	1078	984.2363	30.3834	736.7196	1232	93.5937
10	1231	984.2363	30.3834	736.7196	1232	246.4137
11	618	753.9930	24.2669	509.4140	998.5719	-135.7080
12	780	753.9930	24.2669	509.4140	998.5719	26.1550
13	702	753.9930	24.2669	509.4140	998.5719	-51.8520
14	694	753.9930	24.2669	509.4140	998.5719	-60.2930
15	464	523.7496	26.5641	278.1404	769.3588	-59.5386
16	432	523.7496	26.5641	278.1404	769.3588	-91.5406
17	468	523.7496	26.5641	278.1404	769.3588	-55.7366
18	244	272.5750	36.7076	21.3788	523.7712	-28.6950
19	236	272.5750	36.7076	21.3788	523.7712	-36.4630
20	291	272.5750	36.7076	21.3788	523.7712	17.9770
21	111	63.2628	47.8781	-195.9395	322.4652	47.3022
22	106	63.2628	47.8781	-195.9395	322.4652	42.3092
23	137	63.2628	47.8781	-195.9395	322.4652	73.5222
24	.	963.3051	29.5656	716.2171	1210	.

The above Table 2.7 shows the dependent or response variable *Y*, i.e., the maximum compression load is predicted by the independent variable *X*, span-length. The table displays the results of predicted and residual values; for each observation, the requested information is shown. In this case, row highlighted in red indicates the maximum compressive load (predicted value) for 39 mm span length interpolated to 1210 N. The ID variable is used to identify each observation; for observations with missing dependent variable, the predicted value, standard error of the predicted value, and confidence interval for the predicted value are still available.

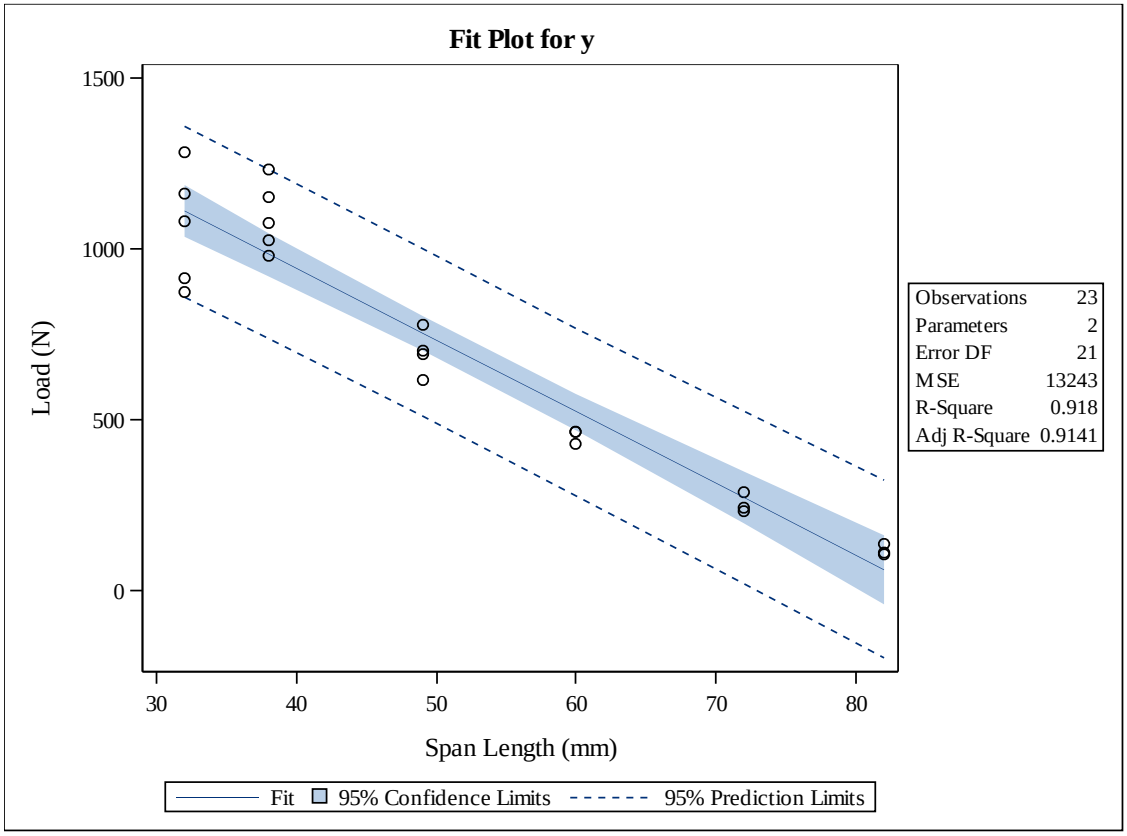

Figure 2.22: Fit plot for maximum compression load, 'y'

Figure 2.22 displays the fit plot induced by the SAS code. The fit plot shows the negative slope of the fitted line. The average compression load on the yarn changes by $\widehat{\beta_1} = -20.931$ N for each millimeter change in span-length. The 95% confidence limits in the fit plot are pointwise limits that cover the mean weight for a particular span-length with probability 0.95. The prediction limits, which are wider than the confidence limits, show the pointwise limits that cover a new observation for a given height with probability 0.95.

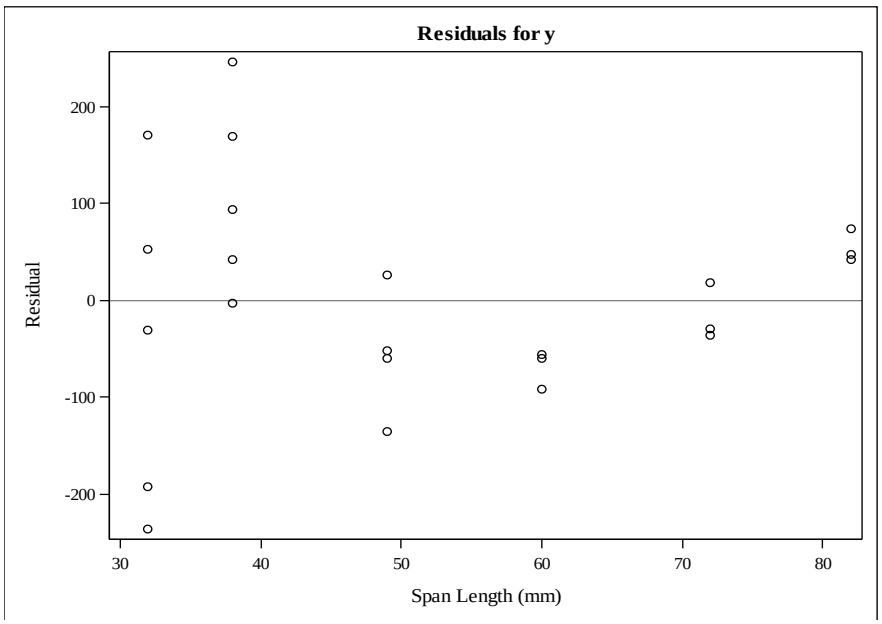

Figure 2.23: Residual for maximum compression load, 'y'

Conclusion

A strong negative linear relationship between the increase in span-length and maximum compressive load carrying capacity of the carbon fiber braided yarn #6 was found with a Pearson's correlation coefficient of -0.95812.

Simple Linear Regression equation obtained for compression load and is given by,

Maximum Compressive Load = 1779.6 -20.931*Span-length.

Some of the assumptions made during the statistical study are that a linear relationship exists between the variables – span-length and maximum compressive load, individual value of maximum compressive loads does not affect the other value of maximum load and equality of variance exists between the variables. However, from Figure 2.23, it was observed that some large residuals (apparent outliers) were present and this indicates that a higher-order model is suitable compared to the linear model carried out in this work. [14]

Thus, based on the large residuals observed in the linear model for a more robust model, a higher order regression model could be used.

Chapter 3
OACS as an Optical Tube on NASA's IROC Satellite

Introduction and Scope of Work

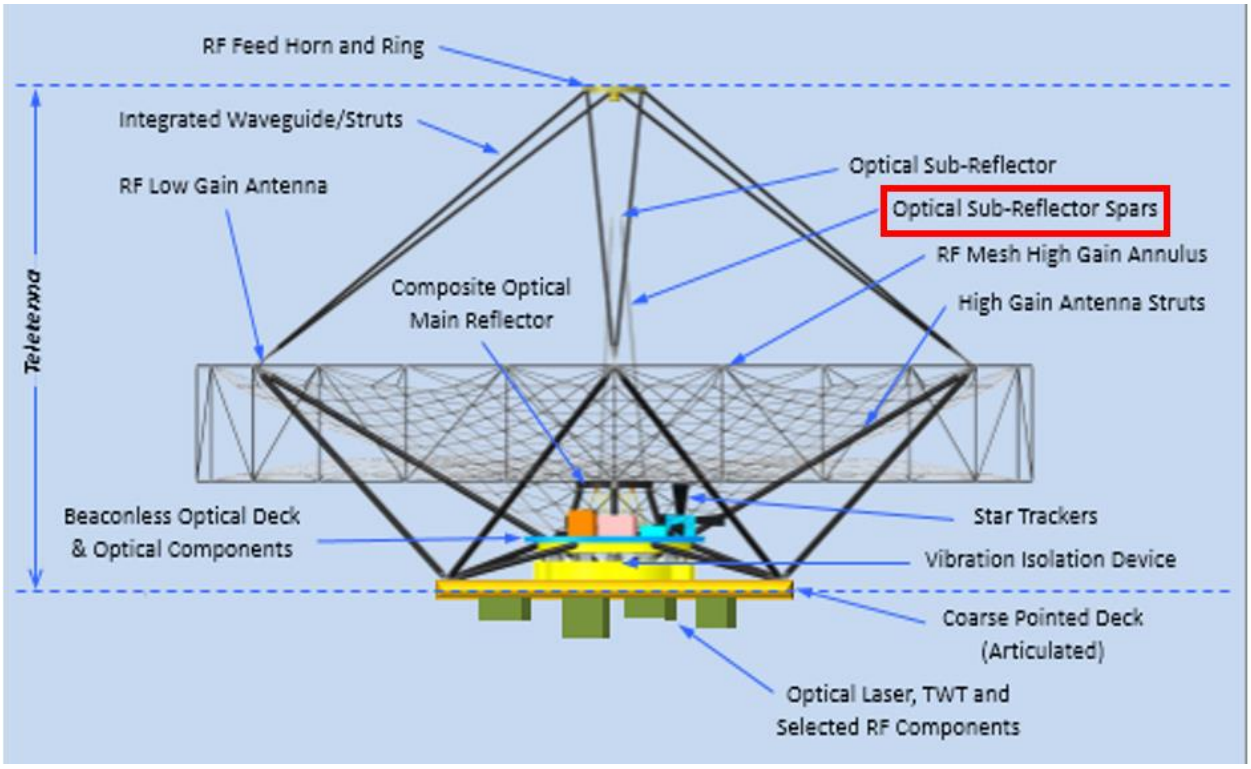

Figure 3.1: Schematic of IROC Satellite, reprinted from [6]

The OACS tube given its open architecture design and stiffness-to-strength ratios might be suitable for the Integrated Radio and Optical Communication (IROC) system and the suitability has been explored in this work. The optical portion of IROC has a 25 cm primary mirror supported on an Optical Bench with a secondary smaller mirror supported 90 cm above the primary mirror. A braided OACS tube as a support structure for the secondary mirror looks like an ideal candidate due to its low mass density, high stiffness, non-metallic properties, low

coefficient of thermal expansion (CTE) and its braided open architecture will help reduce its Radio Frequency (RF) interference.

The ability to braid different patterns and the different ways to accomplish the same goal of a stiff, low mass, stable, and low CTE support for the secondary mirror, provides further application possibilities.

Dimension Requirements for the Optical Tube

Height = 900 mm

Diameter = 280 mm. The I.D must be able to mount a 250 mm O.D. mirror at bottom.

Early path finder could be of smaller diameter of 100 to 150 mm

Must provide solid ring fittings for each end for mounting purposes.

Mass and Stiffness Requirements

Desired Mass < 2 kg

Desired 1st Bending Natural Freq > 100 Hz.

Non-structural mirror supported at top ~ 1kg

RF transparency

RF transparency is critical towards the top of the structure and lower braid density and glass-fiber helical yarns might be able to reduce RF blockage.

As part of this research thesis, the dimensional, stiffness, and mass requirements have been addressed, with further work to be completed by the research group.

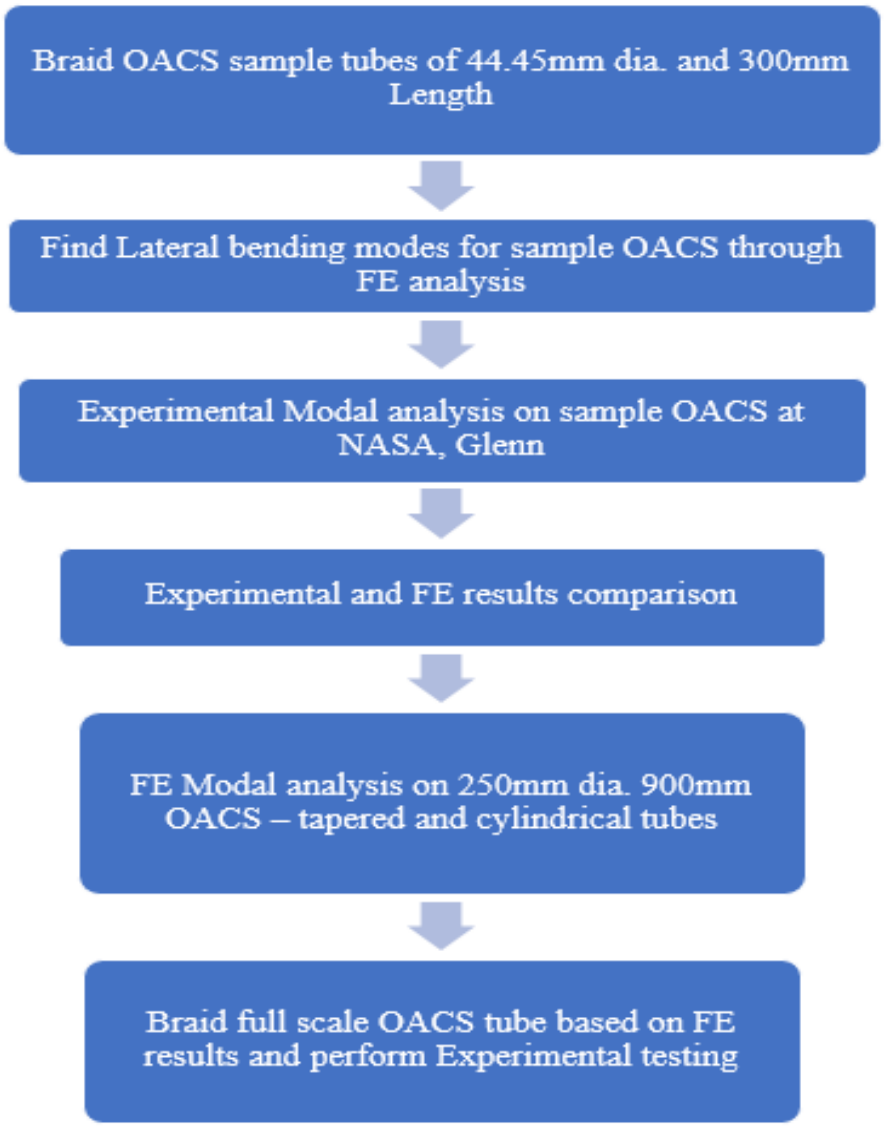

Figure 3.2: IROC-OACS process flow

Compressive Stiffness Test of OACS Structures

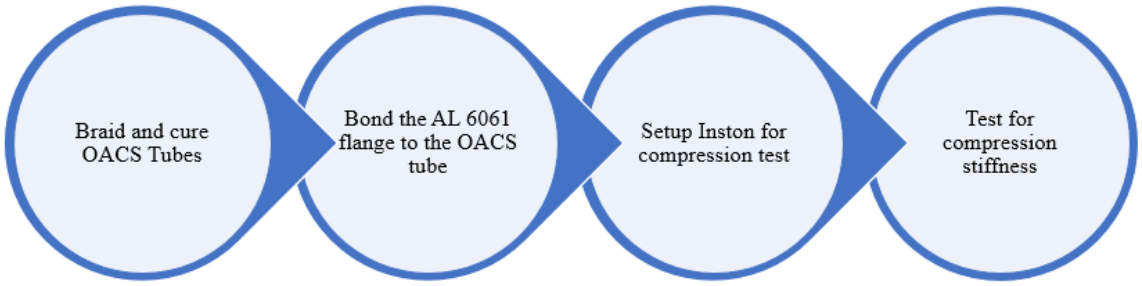

Figure 3.3: Compression Test process flow

Figure 3.4: OACS Specimen

The OACS tubes in Figure 3.4, were tested for their compressive stiffness to understand the difference in all-carbon, all-glass, hybrid tubes.

OACS tubes with carbon fiber axial and helical yarns are referred as “all-carbon”; tubes with glass-fiber axial and helical yarns referred as “all-glass,” and tubes with carbon axial and glass helical yarns are referred as “hybrid tubes.” Table 3.1 has details about the number of yarns,

material of the yarn and helix angle of the OACS tubes that were tested for compressive stiffness.

Table 3.1: Stiffness test specimen

Sl. #	Material-Axial Yarn	Material-Helical Yarn	Axial yarn count	Helical yarn count (CW+CCW)	Helix angle
1.	Glass Fiber	Glass Fiber	6	8	45
2.	Glass Fiber	Glass Fiber	6	8	30
3.	Carbon Fiber	Glass Fiber	6	8	30
4.	Carbon Fiber	Carbon Fiber	6	8	30

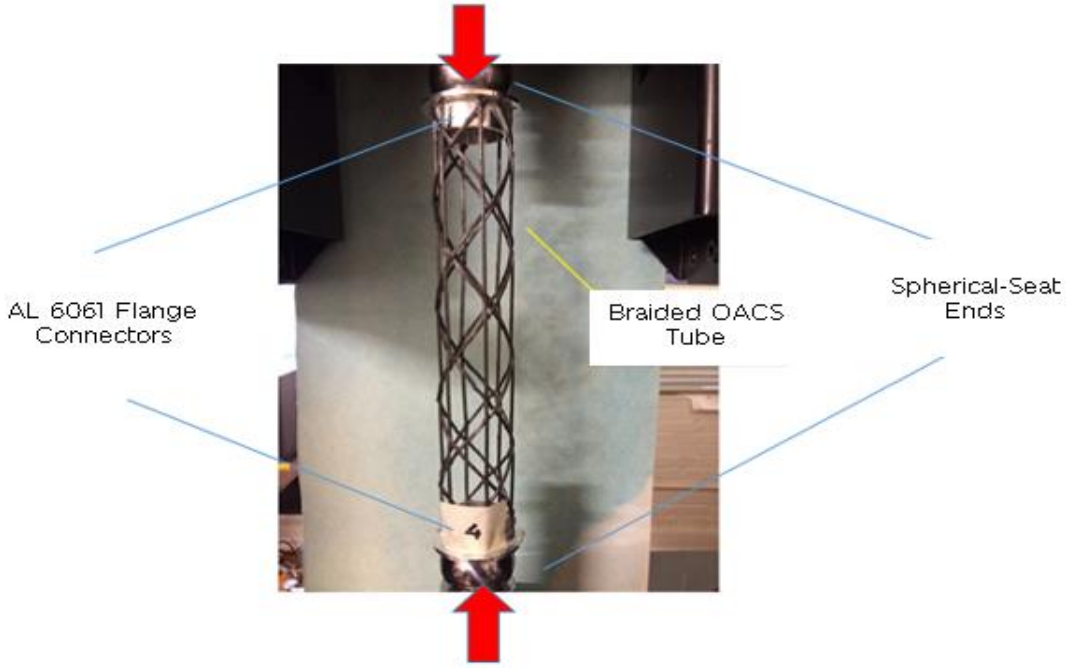

Figure 3.5: OACS tube under compression

The OACS diameter of all structures was 44.45 mm. and the length was 300 mm. Two AL 6061 end connectors were bonded to the OACS tube with 3M DP460 adhesive and cured for 24 Hours at room temperature [13]. To maintain axial alignment during compression loading, the end connectors on the OACS tubes were designed to accommodate 1.375" diameter hardened spherical ball bearings and they were mounted on the Instron 5500 attachment. The compression test speed parameter was set to 3 mm/min.

Table 3.2: OACS Tubes Stiffness comparison table

OACS Structure	Helix Angle in ° D	Span-length (mm.)	Mass (g.)	Compressive Stiffness (N/mm)	% Lighter than Glass Fiber (1)	% Stiffer than Glass Fiber (1)
All Glass Fibers (1)	45	25	40.99	2169.1	0	0
All Glass Fibers	30	50	34.11	2463.2	16.79	13.56
Helical: Glass Fiber Axial: Carbon Fiber	30	60	29.49	4964.7	28.06	128.90
All Carbon Fiber	30	55	25.85	5934.6	36.94	173.59

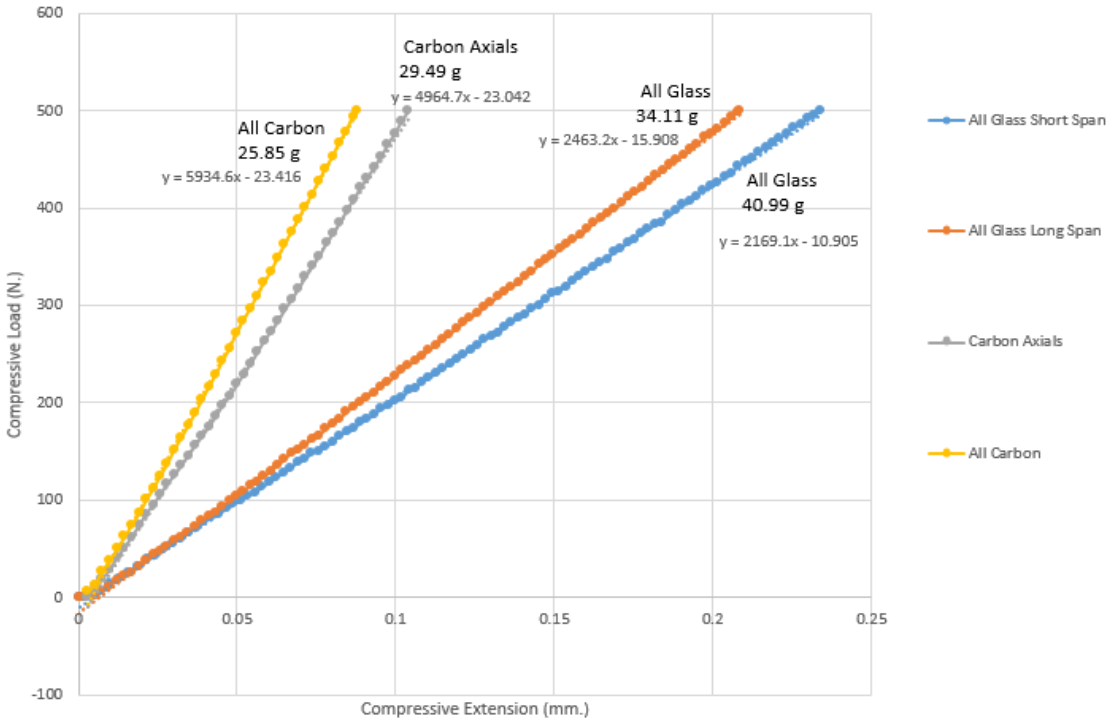

Figure 3.6 Stiffness Comparison of OACS tubes

The experimental test results in Figure 3.6 shows that the OACS tube with all-carbon yarns is about 2.73 *times* stiffer in compression and about 36% lighter when compared to an all glass OACS tube.

The hybrid OACS tube with carbon-fiber axial yarns and glass-fiber helical yarns is about 2.28 *times* stiffer in compression and 28% lighter than the all-glass OACS tube. The hybrid tube might be able to have better RF transparency when compared to the all carbon tube and maintain high compression and lateral bending stiffness due to the carbon fiber axial yarns.

FE-Modal Analysis on All-Carbon-Fiber and All-Glass-Fiber OACS

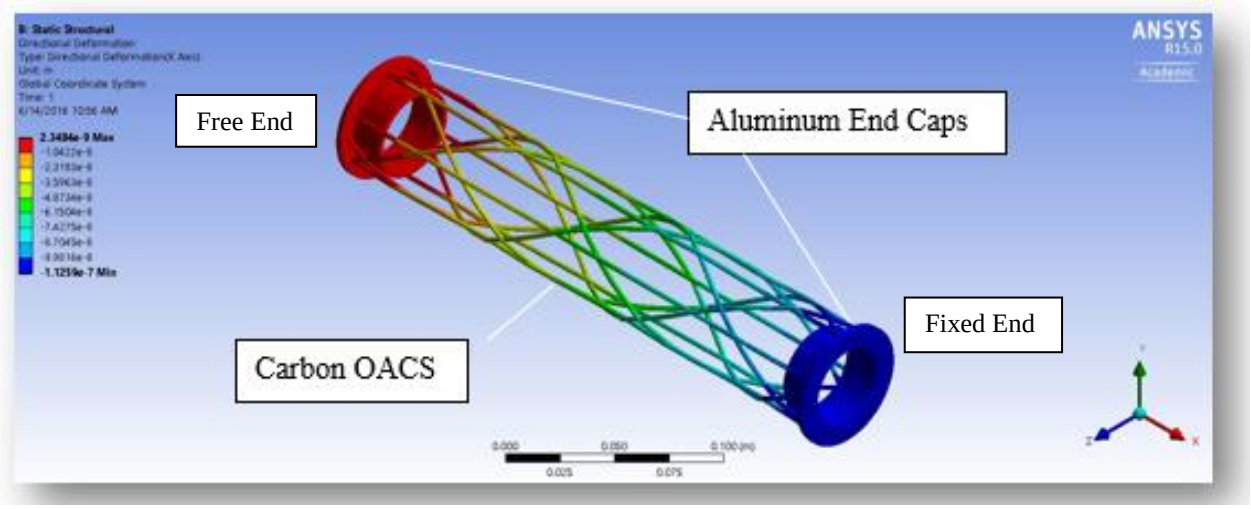

Figure 3.7: Carbon fiber OACS – Cantilever Boundary Condition

The Finite element model of the OACS tubes were modeled as per the physical OACS tubes which was experimentally tested for the first lateral bending mode at NASA Glenn. The tubes tested for 1st lateral bending modes are all in the cantilevered configuration. All-carbon, all-glass and hybrid OACS tubes were modeled with material properties, boundary conditions and physical dimensions as per the physical specimen whose lateral bending modes were experimentally tested.

The initial OACS sample tested both experimentally and by FE method was a cylindrical OACS tube with either all carbon or all glass fiber yarns. The diameter of the OACS tube was 44.45 mm, and the length was 300 mm. The dimensions of the OACS tubes were based on the manufacturing availability of materials and mandrels for braiding multiple test specimen.

The OACS tube had two aluminum rings made of 6061 alloy material; the rings were bonded to the braided structure with 3M DP460 epoxy adhesive. The rings aid in physically clamping the structure for testing without damaging the composite braid.

Modeling and Boundary Conditions of the OACS Tubes

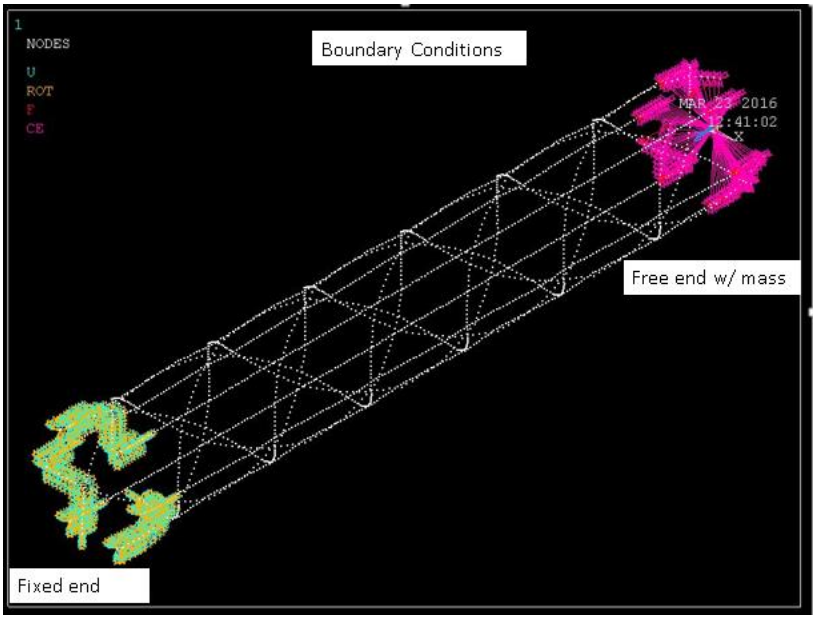

Figure 3.8: ANSYS APDL OACS FE Model

Figure 3.8 illustrates an ANSYS APDL model of the OACS tube. MATLAB *fell_point* code [4] has a user-friendly interface to generate the key points or nodal geometric points of the OACS tubes, once the geometric points were generated, the ANSYS APDL code [11] was used to assign 2-node beam elements of the desired properties and mesh the complete structure. The details of the development of the *fell_point* code can be found in Gurley, et al (Design and

Analysis of Braided Composite Lattice Structures, 2014) [4] and details of the ANSYS APDL code can be found in Yang Shen, et al (Design, Processing, and Failure Analysis of Open-Architecture Composite Structures) [11].

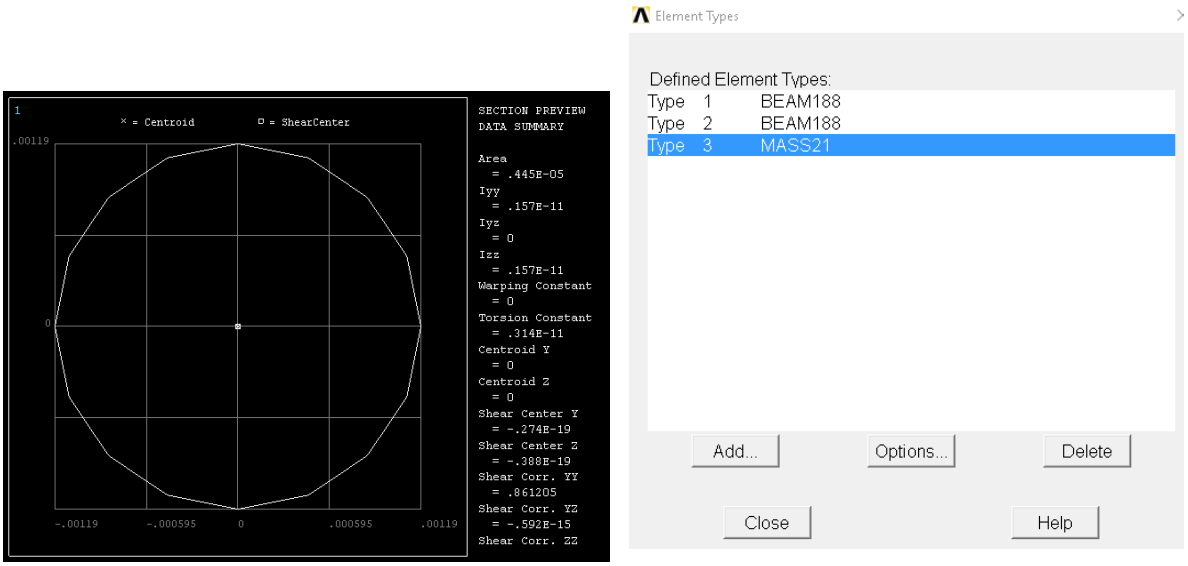

Figure 3.9: ANSYS APDL Element specification

Figure 3.9 illustrates that BEAM188 elements were used to model the OACS tube. The BEAM188 element is suitable for analyzing slender to moderately thick beam structures. This element is based on Timoshenko beam theory. Shear deformation effects are included [15].

BEAM188 is a linear (2-node) beam element in 3-D, each node has six degrees of freedom – They include translations in *x*, *y*, and *z* directions, and rotations about the *x*, *y*, and *z* directions. Warping of cross-sections is assumed to be unrestrained [15].

MASS21 is a point element having up to six degrees of freedom: translations in the nodal *x*, *y*, and *z* directions and rotations about the nodal *x*, *y*, and *z* axes. A different mass and rotary inertia may be assigned to each coordinate direction [15].

The diameters of the yarns from the OACS tubes were physically measured and the cross-sectional area of the beam elements were based on the physical measurements carried out using digital calipers and account for the thickness of the jackets. The diameter of the carbon-fiber yarns was measured to be around 2.38 mm and the glass-fiber yarns were found to be close to 2.40 mm in diameter.

Material Properties for Carbon Fiber and Glass Fiber Yarn

Table 3.3: Orthotropic material properties of carbon-fiber and glass-fiber

	Elastic Modulus (N/m^2)			Poisson's Ratio			Shear Modulus (N/m^2)			Density (Kg/m^3)
Material	EX	EY	EZ	PRXY	PRYZ	PRXZ	GXY	GYZ	GXZ	
Carbon-Fiber	$1.085x10^{11}$	$8.6x10^9$	$8.6x10^9$	0.27	0.4	0.27	$5.0x10^9$	$3.1x10^9$	$5.0x10^9$	1393
Glass-Fiber	$5.0x10^9$	$8.0x10^9$	$8.0x10^9$	0.3	0.4	0.3	$5.0x10^9$	$3.84x10^9$	$5.0x10^9$	2000

The Table 3.3 shows the linear orthotropic material properties for the carbon fiber and glass fibers with EX, EY, EZ being the elastic modulus in N/m^2, GXY, GYZ, GXZ the shear modulus in N/m^2, PRXY, PRYZ, PRXZ the Poisson's ratio. The density of the yarn is given in Kg/m^3, it was obtained by measuring the mass and volume of a cured yarn specimen.

The Young's modulus (*EX*) properties for the carbon fibers were based on experimental test values by Kothari et al (Mechanical Characterization of the Braided Composite Yarn and Bond Strength Evaluation of the Joints of the Open-Architecture Composite Structure (O-ACS), Auburn University, 2014) [7]. The value of 108.5 GPa was a conservative number, with the range for *EX* modulus for unidirectional carbon fibers ranging 100 GPa to 123 GPa.

The material properties for glass fibers were taken from published material library spec. sheet, and ANSYS documentation for unidirectional glass fibers [15].

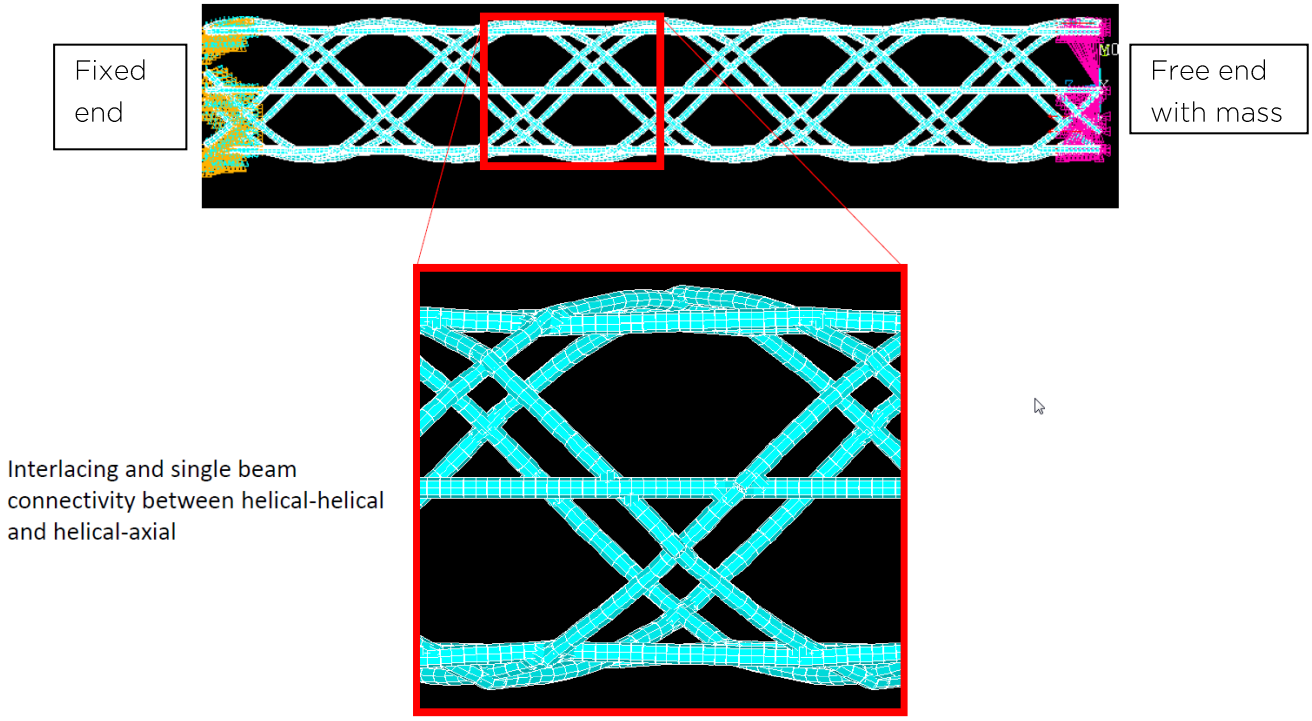

Figure 3.10: BEAM element mesh of the OACS in ANSYS

The loads, boundary conditions, and the mesh refinements were all input in the ANSYS APDL code and were similar to the real world experimental tests carried out at NASA Glenn [6]. The objective was to determine the first modal frequency in the cantilevered configuration – this configuration was chosen based on the application of the OACS tube loaded in this manner.

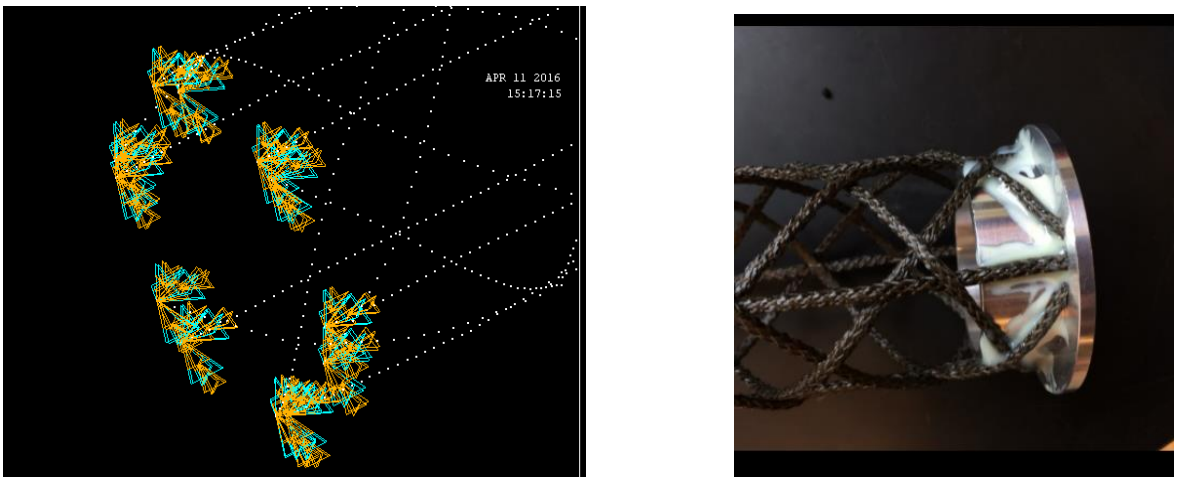

Figure 3.11: Modelling of Aluminum flange - Boundary condition

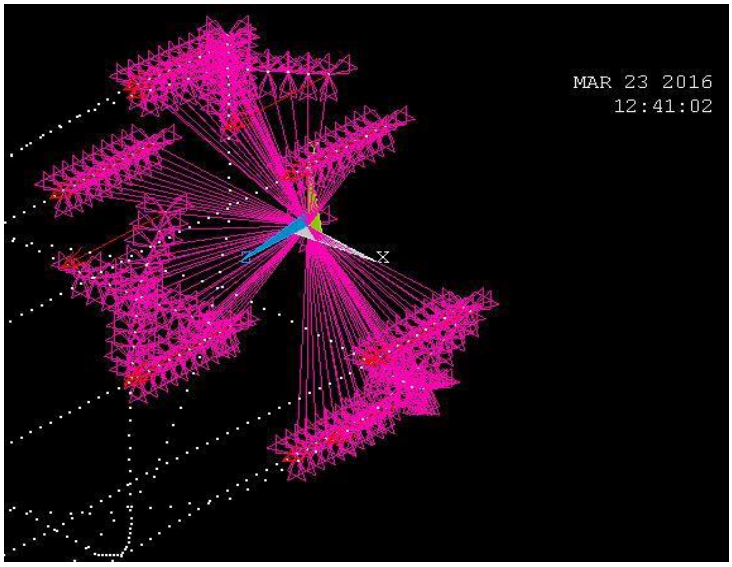

Figure 3.12: FE Modelling of end mass

The flange ends are completely constrained with UX, UY, UZ and ROTX, ROTY, ROTZ on one end which represents the aluminum fixed end as shown in Figure 3.11. The other end of the tube, represented in Figure 3.12 has a rigid coupled-mass mesh with MASS21 elements which represents the mass of the mirror as per of the design requirements.

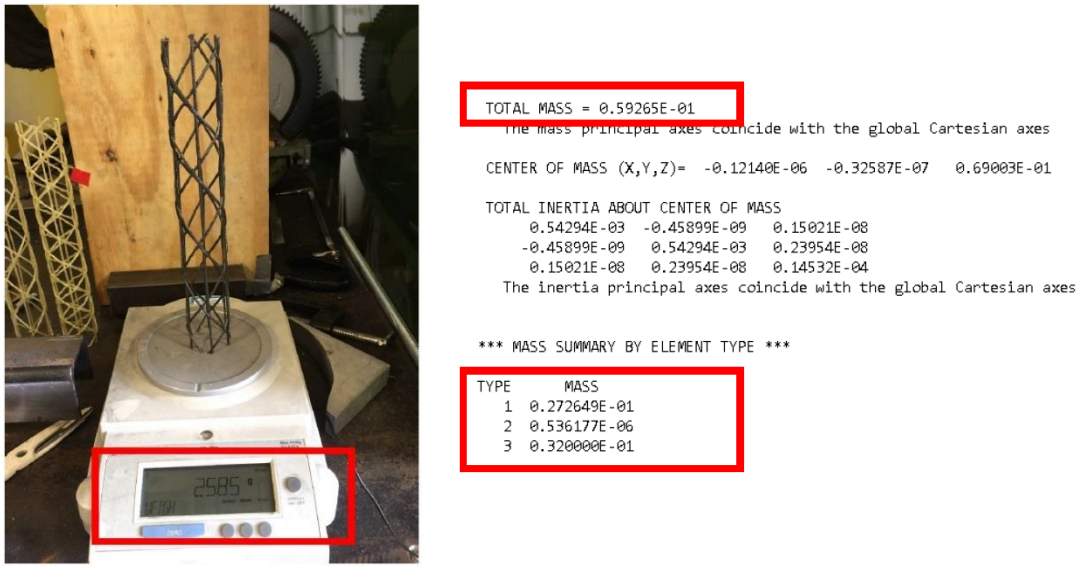

Figure 3.13: OACS Mass measurement for FE modelling

The mass of the physical model was measured and the finite element model was modeled based on the experimental stiffness and mass obtained from the actual physical model.

For the FE analysis, the mass of the aluminum end cap was applied to the nodes at the free end (single only), bringing the total mass to ~60 g.

1. [27.26 g.] –Mass of the helical and axial beam elements

2. [0.5 e-3 g.] –Mass of the joints

3. [32 g.] –Mass of the aluminum end cap

The total mass of the measured OACS tube was found to be 25.85 grams and the FEA model had a 27.265 grams; an approximately 5% difference.

Initial Test Sample 44.45 mm Diameter 300 mm Long, All-Carbon-Fiber OACS

A Conventional Triaxial braid was chosen for the OACS to have better control over the straightness of axial yarns during manufacturing stage. The structure had 4 clockwise helical yarns and 4 counter clockwise helical yarns, 6 axial yarns, a 60^{o} helix angle. The yarns were braided with 72K core carbon fiber tows and a true triaxial braid jacket [12] (2.38 mm measured OD).

OACS All-Carbon-Fiber Modal Results

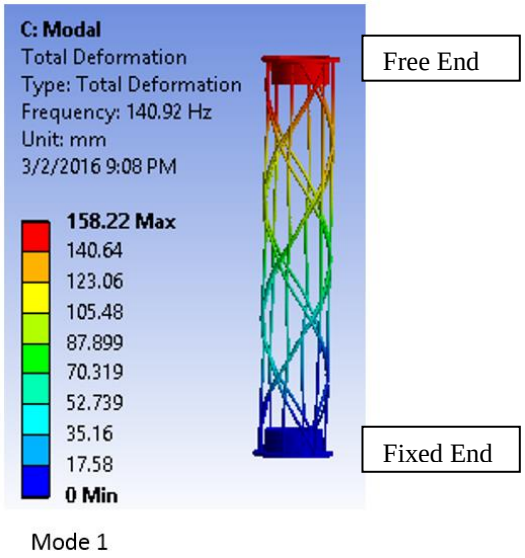

Figure 3.14: Mode 1 – lateral bending all-carbon- fiber OACS tube (Cantilevered Condition)

Table 3.4: Carbon OACS Modal results

MODE	Frequency in Hz.
1	141.69
2	368.96
3	525.3
4	727.98

The FE modal analysis carried out on the initial OACS tube for the IROC project with 44.5 mm diameter and 300 mm length indicates a 1st lateral bending mode of 141.69 Hz. for the all-carbon-fiber yarn for a cantilevered type of boundary condition excited at the free end. The values obtained from the FE analysis have been compared with the experimental results in the following sections.

Initial test sample 44.45 mm diameter 300 mm long – All-Glass-Fiber OACS

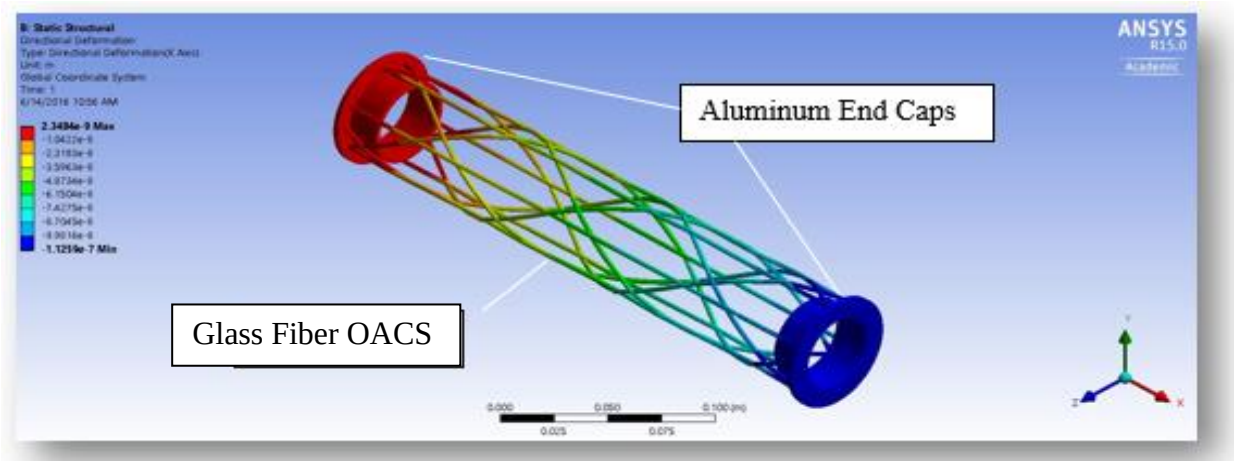

Figure 3.15: Glass-fiber OACS

A Conventional Triaxial braid was chosen for the OACS to have better control over the orientation of axial yarns during manufacturing stage. The structure had 4 clockwise helical yarns and 4 counter clockwise helical yarns, 6 axial yarns with a 45^{o} helix angle. The yarns were braided with glass fibers, 2.40 mm measured OD.

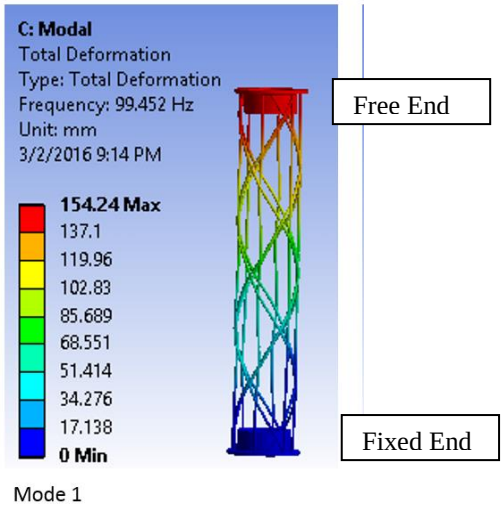

Figure 3.16: Mode 1 lateral bending all-glass-fiber OACS tube (Cantilevered Condition)

Table 3.5: Glass OACS Modal Results

MODE	Frequency in Hz.
1	99.98
2	311.50
3	413.90
4	494.67

The FE modal results from Table 3.5 indicate a 1st lateral bending mode of 99.45 Hz., for the all-glass-fiber yarn OACS tube in a cantilevered type of boundary condition.

The FE modal analysis results for the 44.45 mm diameter, 300 mm long OACS tubes were compared to with experimental test data in the next section and based on the results obtained from this method, modeling of larger OACS tubes with 250 mm diameter and 900 mm length was carried out.

OACS Experimental Modal Survey - NASA Glenn - Ref. [6]

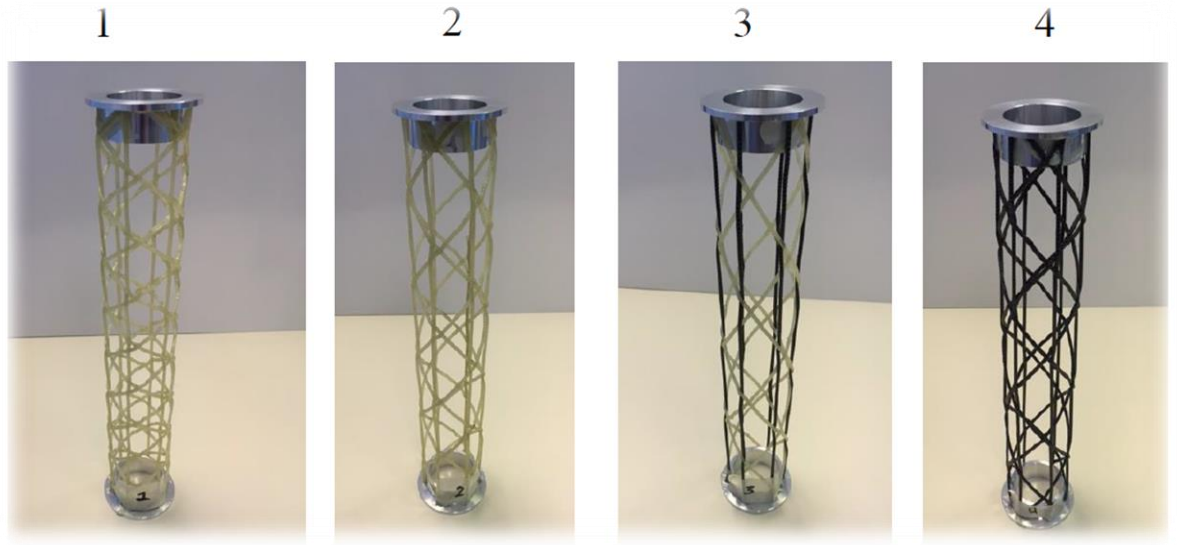

Figure 3.17: Experimental Modal IROC-OACS test specimen

Figure 3.17 shows different configurations of the OACS tubes which were initially tested for 1st lateral bending frequency at NASA Glenn. The physical dimensions of the tubes remain the same however, the helical angle, and the yarn material were different.

Table 3.6: Experimental Modal IROC-OACS Test specimen specification

Sl. #	Material- Axial Yarn	Material- Helical Yarn	Helix angle
1.	Glass Fiber	Glass Fiber	45
2.	Glass Fiber	Glass Fiber	60
3.	Carbon Fiber	Glass Fiber	30
4.	Carbon Fiber	Carbon Fiber	30

Table 3.6 shows different OACS tube configurations with differences in material of the yarn and the change in helix angle. Four OACS tubes 44.45 mm in diameter and 300 mm long were subjected to experimental modal analysis to identify their respective 1st lateral bending modes. The goal of this test was to compare NASA-Glenn's [6] experimental modal values with that of

Auburn University's, and the author's FEA results in preparation to scale up and predict the modal behavior of much larger OACS-tubes.

Boundary Condition – Experimental Modal Analysis

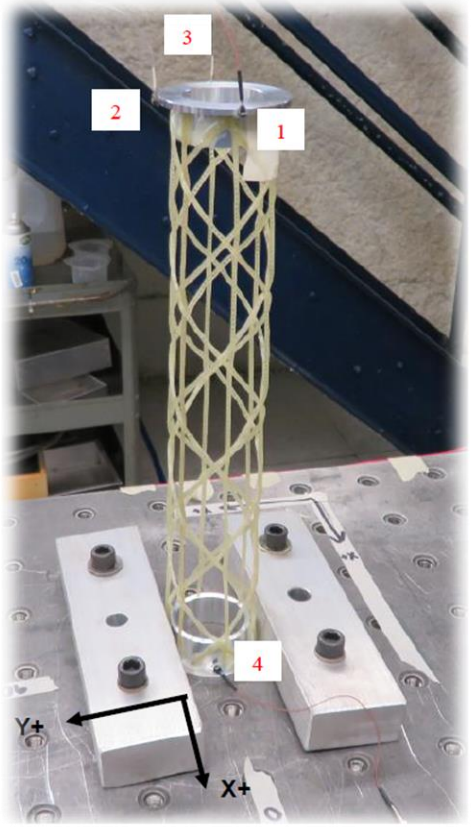

Figure 3.18: Modal Test fixture; reprinted from [6]

Figure 3.18 illustrates the physical mounting of the structure which was carried out by clamping the aluminum end connectors with two pieces of AL bar stock and 5/16" fasteners were used to clamp down the assembly on the C60 shaker clip table. The bolts were torqued down to 12 ft-lbs and the resulting condition was that of two modal surveys per tube and two drive points on the top flange could be recorded.

Accelerometer Placement

Invalid modal frequencies that are less than the actual frequencies are produced due to mass loading effect, to avoid the mass loading effects, lightweight Endevco 22 charge type accelerometers and Unholtz-Dickie charge amplifiers were used.

Four accelerometers were used with the assuming the fundamental motion as global lateral bending. Oval-ing of the top flange would be captured by the two opposing accelerometers. The rocking motion of the bottom flange would be captured by the vertical accelerometer.

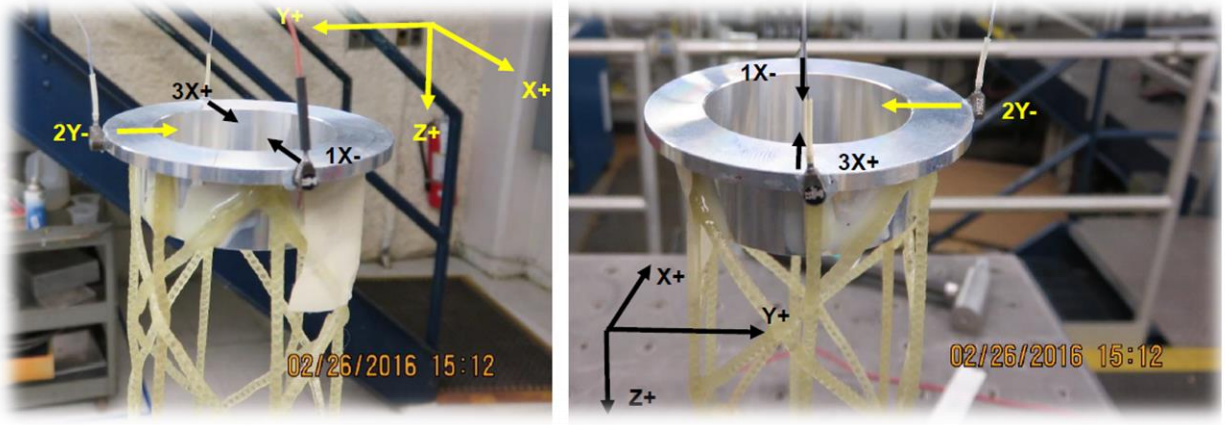

Figure 3.19: Accelerometer mounting; reprinted from [6]

Bee's wax was used to mount the accelerometers. Coordinate system was fixed to the mounting base. It did not change with the orientation of the tube.

The four accelerometers, each at a unique location were used:

Top Flange: 0° Location: 1X-

Top Flange: 90° Location: 2Y-

Top Flange: 180° Location: 3X+

Bottom Flange: 0° Location: 4Z+

Modal Excitation – Impact Hammer Drive Point Locations

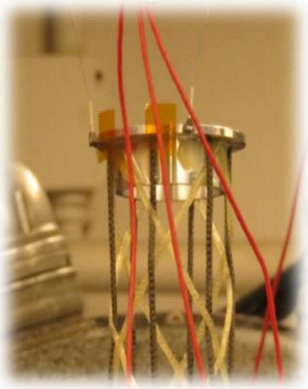

Figure 3.20: Impact hammer drive point location; reprinted from [6]

A PCB model 086E80 miniature modal hammer with a metal tip was used for all surveys. The two impact locations on the top flange were used for all surveys. 90° (2Y-) location; 180° (3X+) location. Kapton tape was put down at the two impact locations to ensure the modal hammer was electrically isolated from the accelerometers.

Data Acquisition Setup & Processing

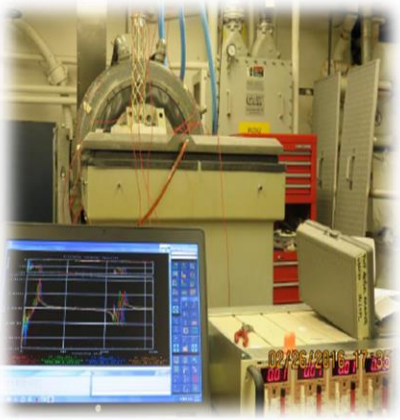

Figure 3.21: Data Acquisition; reprinted from [6]

IDEAS-Test software was used to collect the test data with B&K LAN-XI data acquisition front end hardware. Sampling frequency of 4096 Hz yielding a maximum frequency of 1600 Hz.

IDEAS - Test and B&K Pulse Reflex used to post process the acquired time histories into PSD's, coherence, and FRF. Ideas-Test and B&K Pulse Reflex used to extract modal parameters.

Ten individual impacts were acquired at each drive point location. Tubes #2 – #4 data was acquired using a 1s frame length resulting in a 1 Hz. spectral resolution. Tube #1 data was acquired using a 2s frame length resulting in a 0.5 Hz spectral resolution

Test Methodology

To determine the repeatability and variance in the experimentation procedure, each tube was tested twice.

Test Orientation #1

Placed flange #1 on top and flange #2 on the bottom in the clamps. Based upon how it was mounted on the table. Carried out two impact tests. One drive point location was at 180° (3X+) and the other was at 90° (2Y-).

Test Orientation #2

The tube was rotated 180° around the Y axis, so that the flange #1 was now clamped at the base, and the flange #2 was on top and tapped on. Arrows were marked at X and Y axes on flange #2. Carried out two impact tests. One drive point location was at 180° (3X+) and the other was at 90° (2Y-).

Naming convention of the Modal tests

IROC_BM_Tube#_ImpactLocationDegrees_TestOrientation#

Example: IROC_BM_2_180_02 is the second IROC tube that was impacted in the 180° (3X+) location on Test Orientation #2 of the tube.

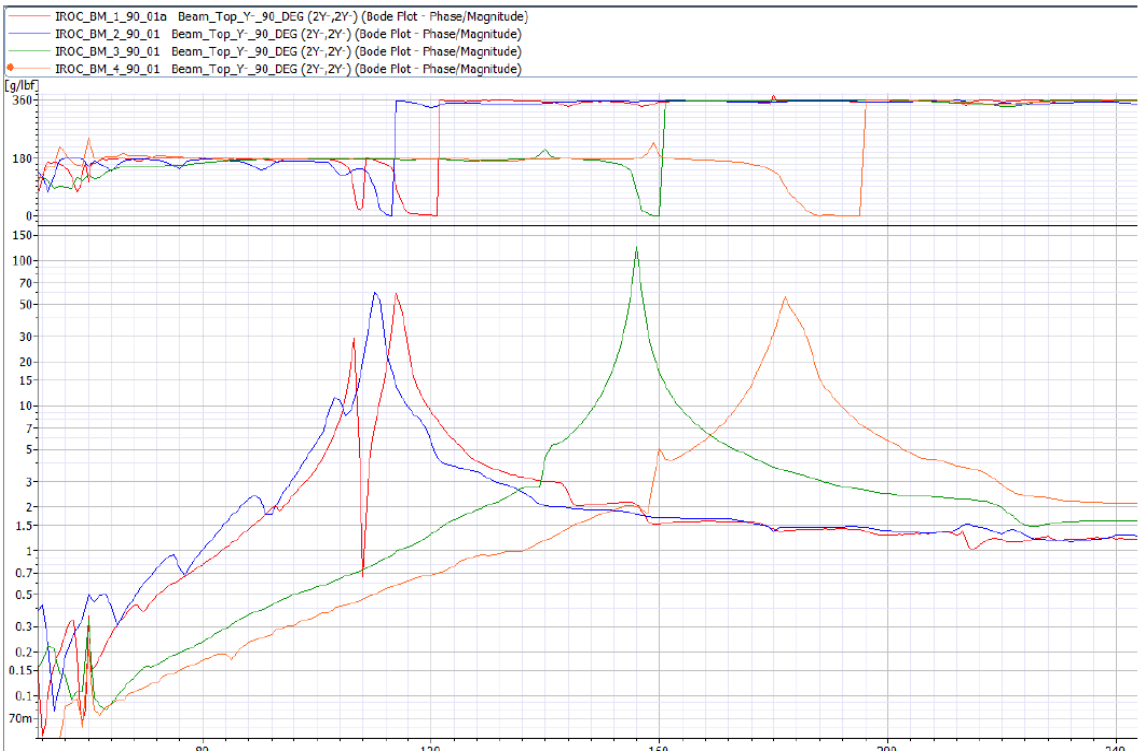

Figure 3.22: All Tubes, 90° Drive Point Location, Test Orientation 1, 1st Resonance Frequency Grouping; reprinted from [6]

Figure 3.22 shows the frequency response obtained from the accelerometers mounted at various locations on the OACS tube.

The tubes had some variability in frequencies which may be due to the variation in the stiffness of the adhesive joints between the yarns and the flanges, i.e., differences in the amount of yarns bonded to the flanges at the location where the accelerometers were mounted, might have contributed to the variation in the peaks observed.

Table 3.7: Exp. modal results initial IROC test specimen, carried out at NASA Glenn [6]

Sl. No.	Specimen Name	Description	Weight (g.)	1st Bending Mode (Hz.)
1.	All Glass	45° helix angle, both axial and helical Glass yarns	105*	114
2.	All Glass	60° helix angle, both axial and helical Glass yarns	99*	110
3.	Hybrid	30° helix angle, Carbon axial and Glass helical yarns	93*	140
4.	All Carbon	30° helix angle, both axial and helical Carbon yarns	91*	159

*Weight of structure + weight of aluminum alloy potted ends

Conclusion

The first lateral bending modes for the all-carbon-fiber OACS tube with 30° helix angle was experimentally found to be around 159 Hz., and the FE results for the same test yielded a prediction of 149 Hz., approximately 7% difference, and for the all-glass-fiber structure, the experimental lateral bending mode was 114 Hz., compared to the FE results indicated value of 99.45 Hz – a difference of about 13%.

The experimental values were derived from the accelerometers mounted on the top flange of the OACS tube and the accelerometers were not mounted on the individual yarns to map the local deflections.

This test sets a reference for future testing of larger OACS tubes up to 900 mm long and 250 mm in diameter.

Chapter 4
FE Analysis to Find 1st Bending mode of Full Scale OACS Tube

Scope of work

The results from the previous chapter which included the comparison between the experimental and FE 1st bending frequencies of the small OACS tubes measuring, 44.5 mm in diameter and 300 mm in length, led to the modelling of larger, full-scale OACS tubes for the IROC application. This chapter covers the modelling and FE analysis of 250 mm diameter *x* 900 mm long, tapered and cylindrical OACS tubes. The analysis considers varying the yarn diameters, changing the number of axial yarns and helical yarns and the effects of varying helical angles on the 1st bending frequencies of the structure. Figure 4.1 shows the process of flow adopted in this chapter, it illustrates the steps taken in deciding the geometry, modelling the tubes, creating elements, meshing the model and running the analysis.

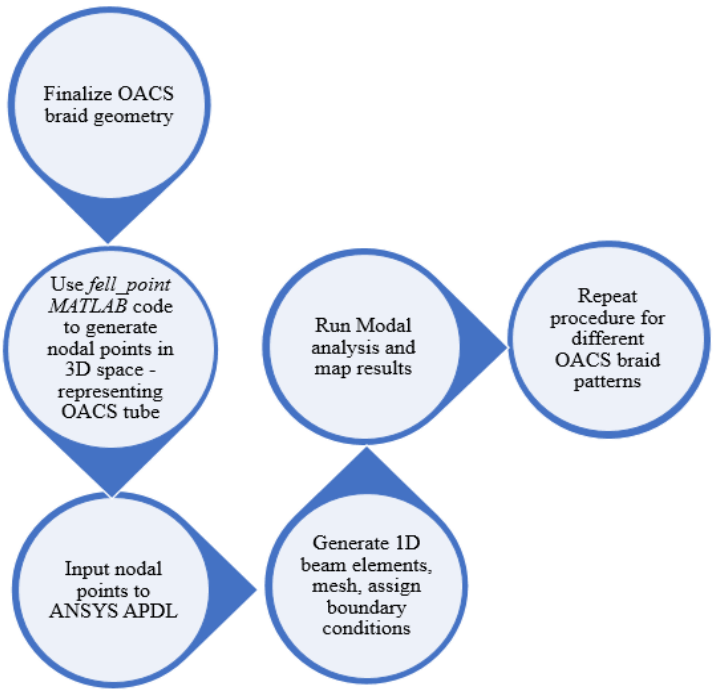

Figure 4.1: FE process flow, IROC-OACS

Naming Convention of OACS Tubes

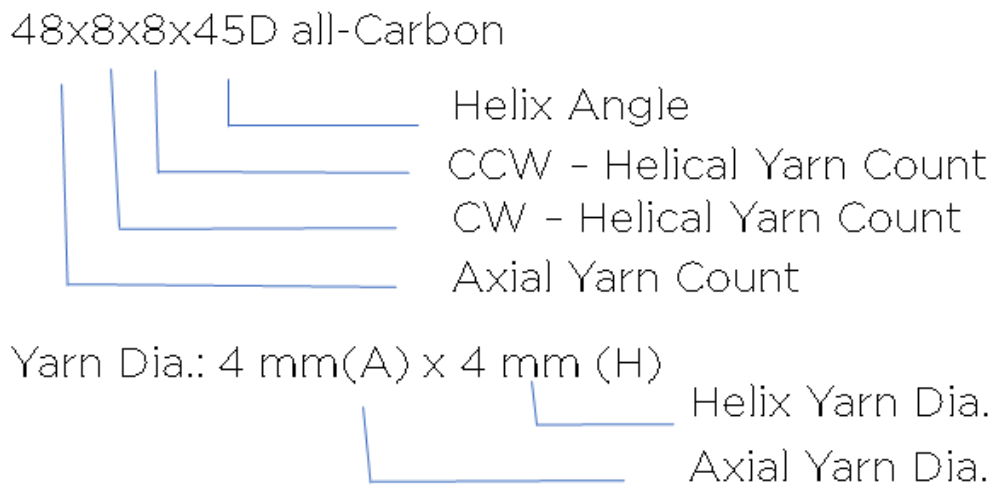

Figure 4.2: FEA naming convention

The Figure 4.2 shows the naming convention of the IROC-OACS tubes followed throughout this analysis. The material of the yarns is specified as all-carbon, all-glass, carbon-fiber axials and glass-fiber helicals (hybrid) for the relevant structures.

FEA of ***Tapered*** or ***Conical*** OACS for IROC Application

From analytical and FE calculations, given the dimensional and mass-stiffness constraints, a conical or tapered geometry of the entire OACS tube had great potential and was investigated to check for the 1st lateral bending frequency. From a bending stiffness stand point, the tapered geometry was about 40% stiffer compared to the cylindrical one [12].

Feasibility with respect to packaging the mirrors and other requirements such are manufacturing ease, thermal expansion, RF transparency, hasn't been considered in this chapter.

Two different types of tapered OACS tubes were modeled based on experimental evidence from previous work which shows that the axial yarns bear the maximum loads when the structure is subjected to compressive and bending loads [4][9]. This is important because, the yarns which take up the maximum loads can be selectively strengthened by increasing their fiber count, there by achieving the maximum strength-weight ratio of the entire structure.

The overall dimension of the structure, i.e., the lower diameter, upper diameter and the height of the structure being fixed, the yarn diameters and the helical angles could be changed.

Increasing the helical angle would result in longer "span-length" of the axial yarns between joints and nodes which increases the chances of failure due to buckling.

The tapered OACS tube configuration analyzed in this work is of 12x6x6 configuration, it consists of 12 axial yarns, 6 clockwise helical yarns and 6 counter clockwise helical yarns.

Two different types of Tapered OACS were subjected FE Modal Analysis:

1. Having equal number of fiber count in both helical and axial yarns.
2. Increasing the fiber count only in the axial yarns since axial yarns are subjected to the highest loads.

Equal Diameter Axial and Helical Yarns – 12x6x6 OACS Tube

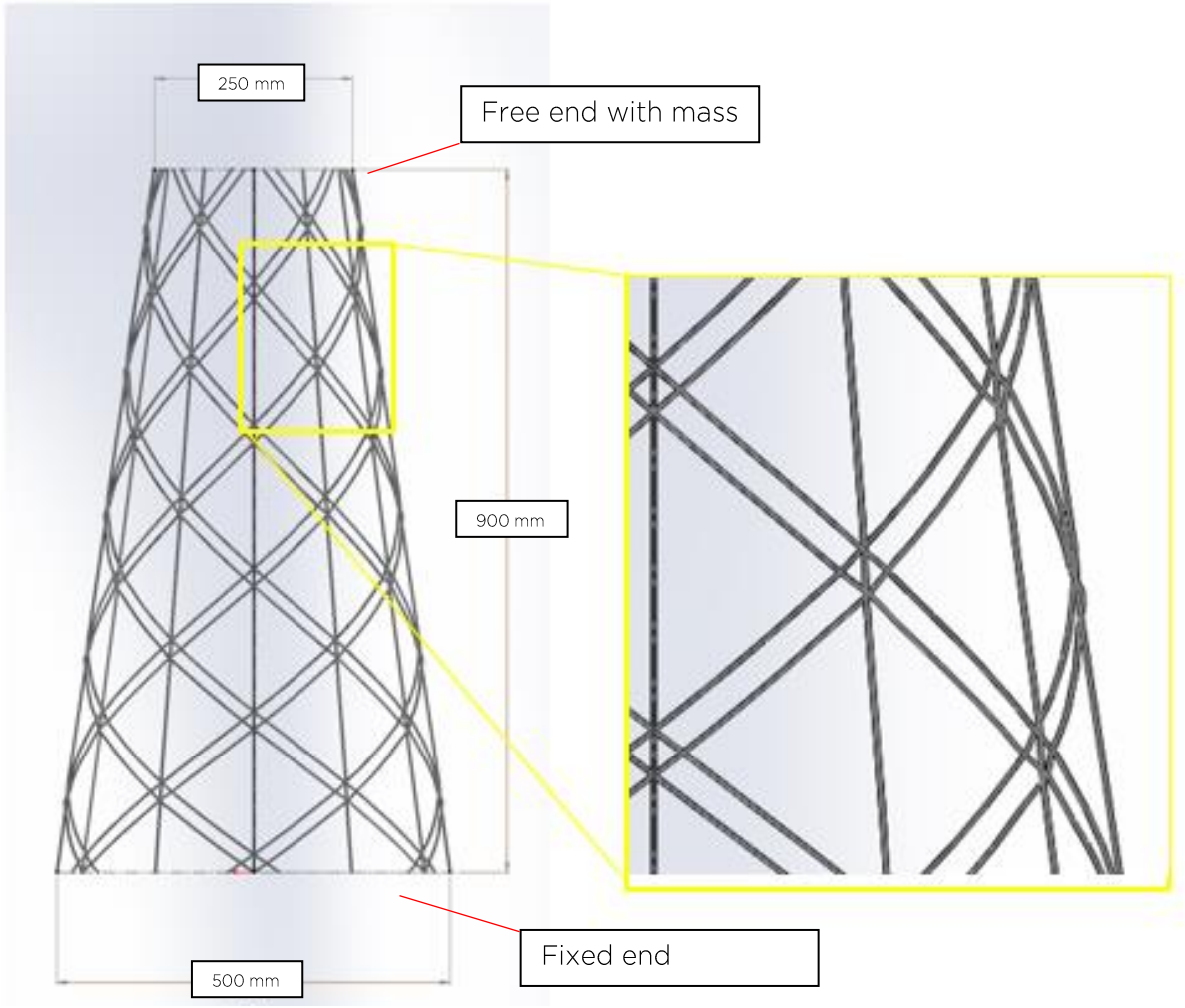

Figure 4.3: Tapered OACS with equal core diameter yarns

As per the requirements, the overall mass of the OACS tube for IROC application had a limitation of 2 Kg., the surface area of the OACS was also an important factor in the overall RF transparency. Given these two important factors, first the tapered 12x6x6 OACS tube with equal axial and helical yarn fiber count was analyzed to understand the behavior of the structure and to obtain 1st lateral bending frequencies. The dimensions of the tapered OACS tube considering the design requirements was, 250 mm smaller diameter, 500 mm larger base-diameter and 900 mm overall length.

Table 4.1: First Modal frequency - Tapered OACS equal diameter yarns (IROC)12x6x6

Core (x1000)	Yarn Dia. (mm.)	OACS Structure Mass (grams)	First Bending Modes (Hz.)
72	2.172	139.096	34
84	2.346	162.24	39
96	2.373	166.097	40
108	2.659	208.521	48
120`	2.803	231.659	52
132	2.940	254.795	56
144	3.070	277.93	60
156	3.195	301.064	64
168	3.316	324.197	68
180	3.432	347.33	72
192	3.545	370.461	75
204	3.654	393.592	79
216	3.760	416.721	82
228	3.863	439.851	85
240	3.963	439.853	85
252	4.061	486.108	91
264	4.156	509.236	94
276	4.249	532.363	97
288	4.341	555.49	100
300	4.430	578.616	103
312	4.518	601.743	105
324	4.604	624.869	108

At 300K yarn core count (about 4.43 mm Diameter), The first mode of 100 Hz. was achieved.

Based on the factors mentioned earlier, multiple iterations were carried out by varying the fiber count in the axial and helical yarns with both helical and axial yarns having the same fiber count.

The required first Mode of over 100 Hz. was achieved with a structure having 300K axial and helical carbon fiber count, the mass of the structure being 579 grams.

Larger Diameter Axial Yarns Compared to Helical Yarns – 12x6x6 OACS

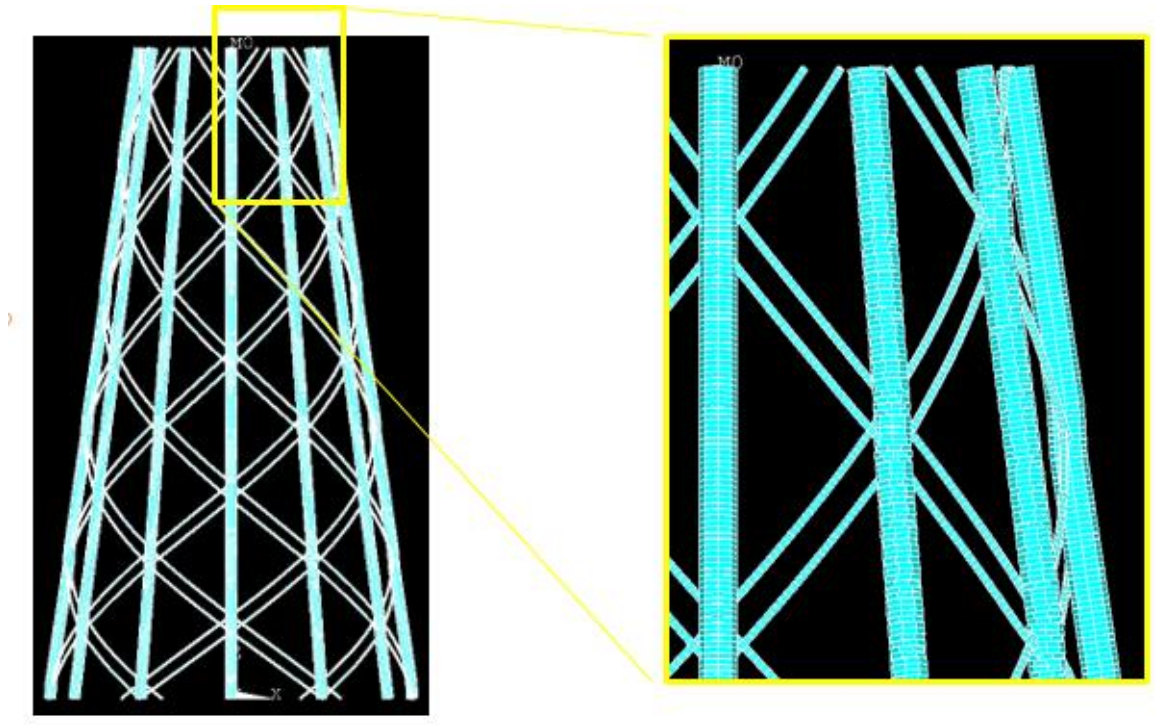

Figure 4.4: Tapered OACS with larger axial yarn diameter

Work carried out by Gurley [4], pointed towards higher loads being transferred through the axial yarns during compression and bending loading, the fiber count in the axial yarns was significantly increased to check for the Modal behavior, compression stiffness and bending stiffness of the Tapered OACS.

Multiple iterations and combinations of fiber count in axial and helical yarns were carried with the objective of achieving the first modal frequency of over 100 Hz., for the structure.

Table 4.2: First Modal frequency - Tapered OACS (IROC)12x6x6

Axial Core (x1000)	Axial Dia. (mm.)	Helical Core (x1000)	Helical Dia. (mm.)	Structure Mass (Kg.)	First Modes (Hz.)
600	6.26	144	3.07	0.633	97.73
600	6.26	192	3.55	0.649	112.34
300	4.43	300	4.43	0.455	95.04
324	4.6	324	4.6	0.472	97.56

After carrying out the Finite Element analysis, Tapered OACS tubes with 600K core axial yarns and 192K core helical yarns with a structural mass of 649 grams has the design stiffness characteristics with 1st bending mode exceeding 100 Hz., and meets the mass and modal requirements for IROC application.

Limitations in capabilities for braiding the 600K carbon core yarns has been explained in the next section, the yarn limitations along with the complexity in manufacturing a 900 mm long tapered aluminum alloy mandrel steered the research in the direction of developing prismatic cylindrical OACS tubes, development details are in the next section

.

FEA of ***Cylindrical*** OACS for IROC Application

From a packaging and manufacturing stand point, cylindrical OACS tube was better able to serve the requirements, and multiple combinations of yarns were modeled and subjected to Finite element modal analysis to find the cylindrical OACS tubes with 1st lateral bending frequencies meeting or exceeding the design requirement of greater than 100 Hz.

48x12x12x60D all 4 mm Diameter Yarns

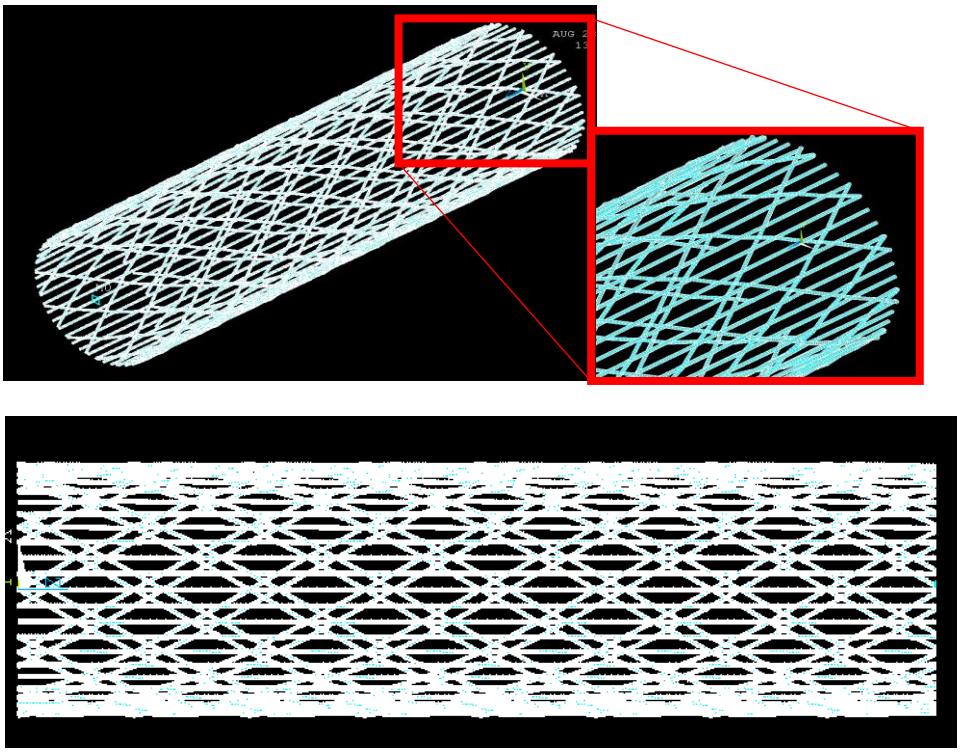

Figure 4.5: Cylindrical IROC - 48x12x12x60D

The above OACS cylindrical structure is 250 mm in diameter and 900 mm long, the axial and helical yarns are 4 mm in diameter and have approximately 252K carbon fiber count.

The number of axial yarns is 48, helical yarn count in clockwise is 12 yarns and helical yarn count in counter-clockwise is 12 yarns, the helix angle is 60^{o}.

48x8x8x45D All 4 mm Diameter Yarns

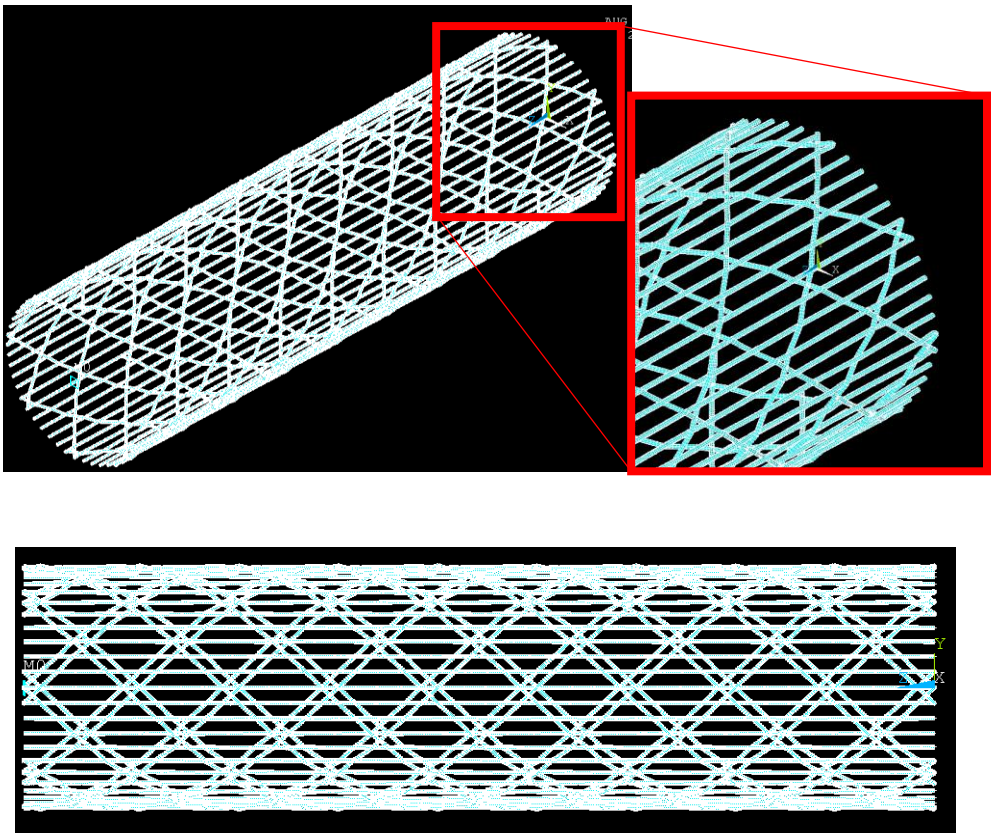

Figure 4.6: Cylindrical IROC - 48x8x8x45D

The above OACS cylindrical structure is 250 mm in diameter and 900 mm long, the axial and helical yarns are 4mm in diameter and have approximately 252K carbon fiber count.

The number of axial yarns is 48, helical yarn count in clockwise is 8 yarns and helical yarn count in counter clockwise is 8 yarns, the helix angle is 45^{o}

48x12x12x45D All 4 mm Diameter Yarns

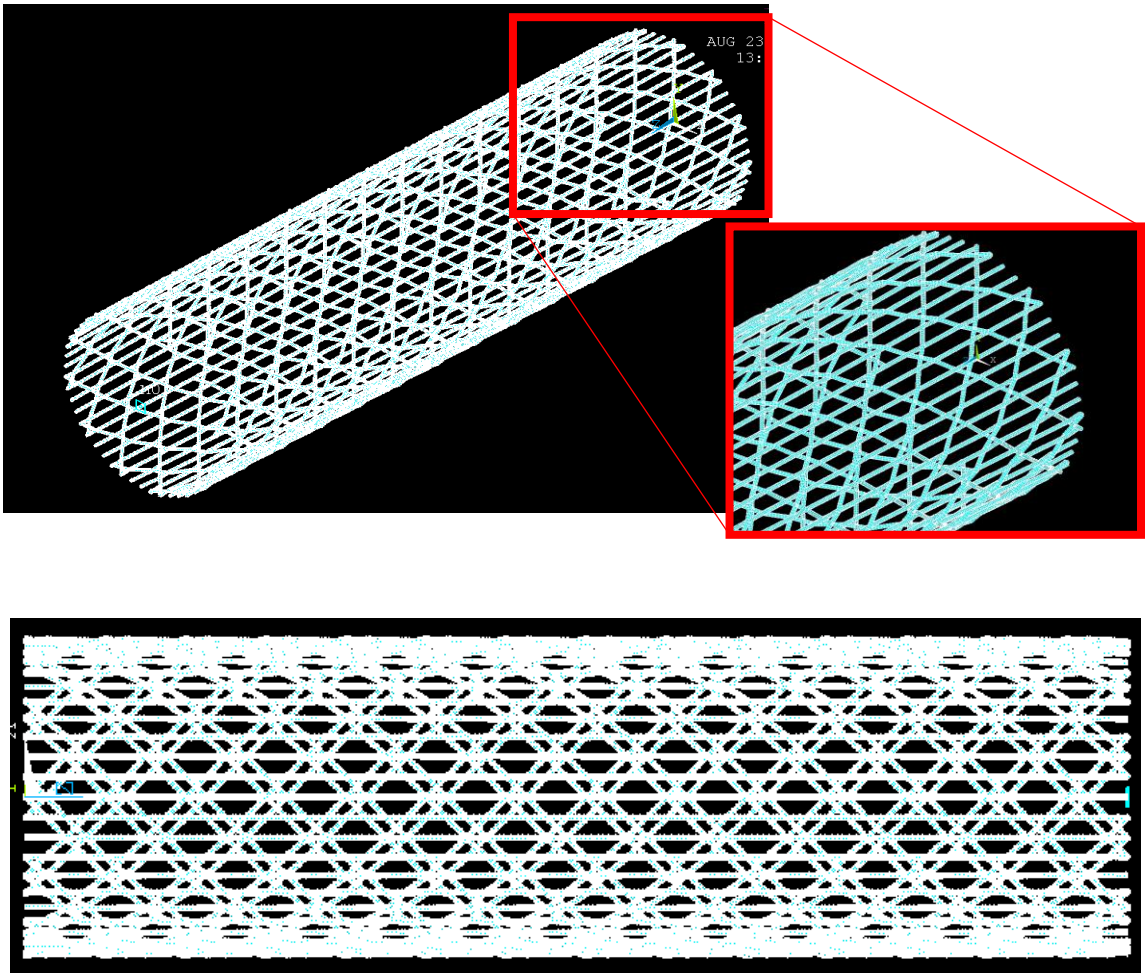

Figure 4.7: Cylindrical IROC - 48x12x12x45D

The above OACS cylindrical structure is 250 mm in diameter and 900 mm long, the axial and helical yarns are 4 mm in diameter and have approximately 252K carbon fiber count.

The number of axial yarns is 48, helical yarn count in clockwise is 12 yarns and helical yarn count in counter clockwise is 12 yarns, the helix angle is 45º.

Design for RF transparency

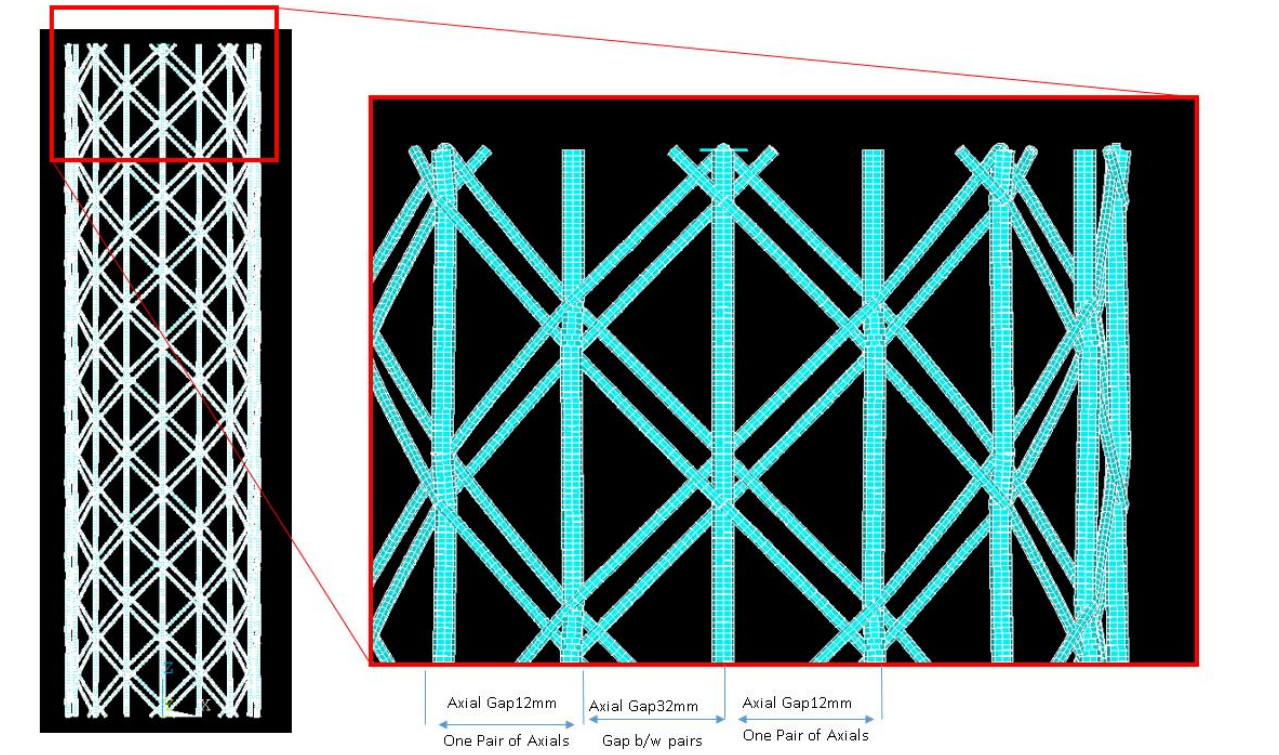

Figure 4.8: "Gap" requirements for RF transparency

The requirements for the IROC structure necessitated the stiffness of the structure not to be compromised when designing the structure for RF transparency. Higher yarn count and acute helix angles contribute to a denser structure thereby limiting the RF transparency for the IROC application. The models created for FE modal analysis accounts for the requirements in “gaps” based on the theory that the “open” nature of the structure would limit the loss in RF signals and improve the efficiency of the IROC satellite.

Visualization of Wireframe - OACS Boundary Conditions and Results

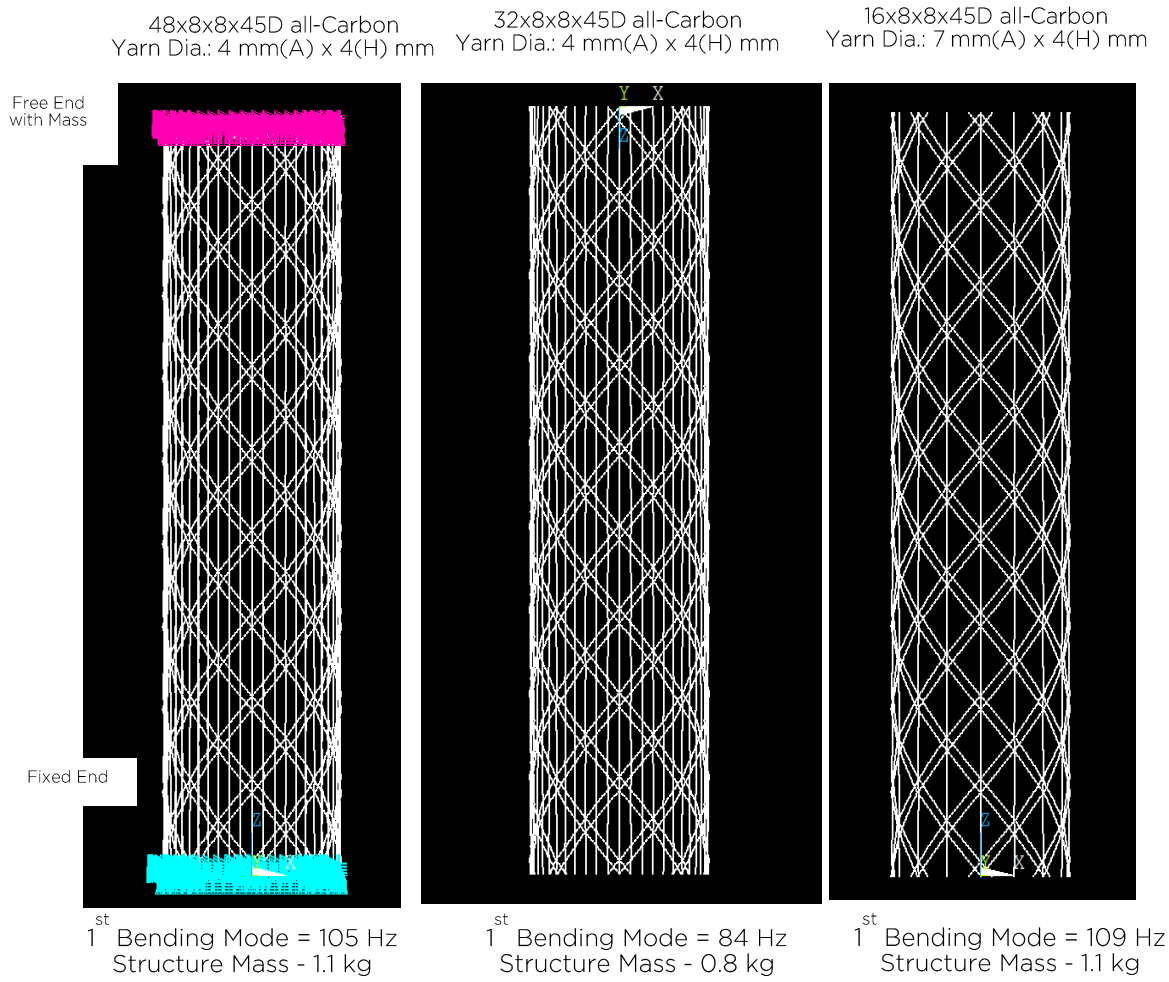

Figure 4.9: Modal Analysis of Cylindrical OACS – all-Carbon

Details about Figure 4.9 and Figure 4.10 are explained in the next page.

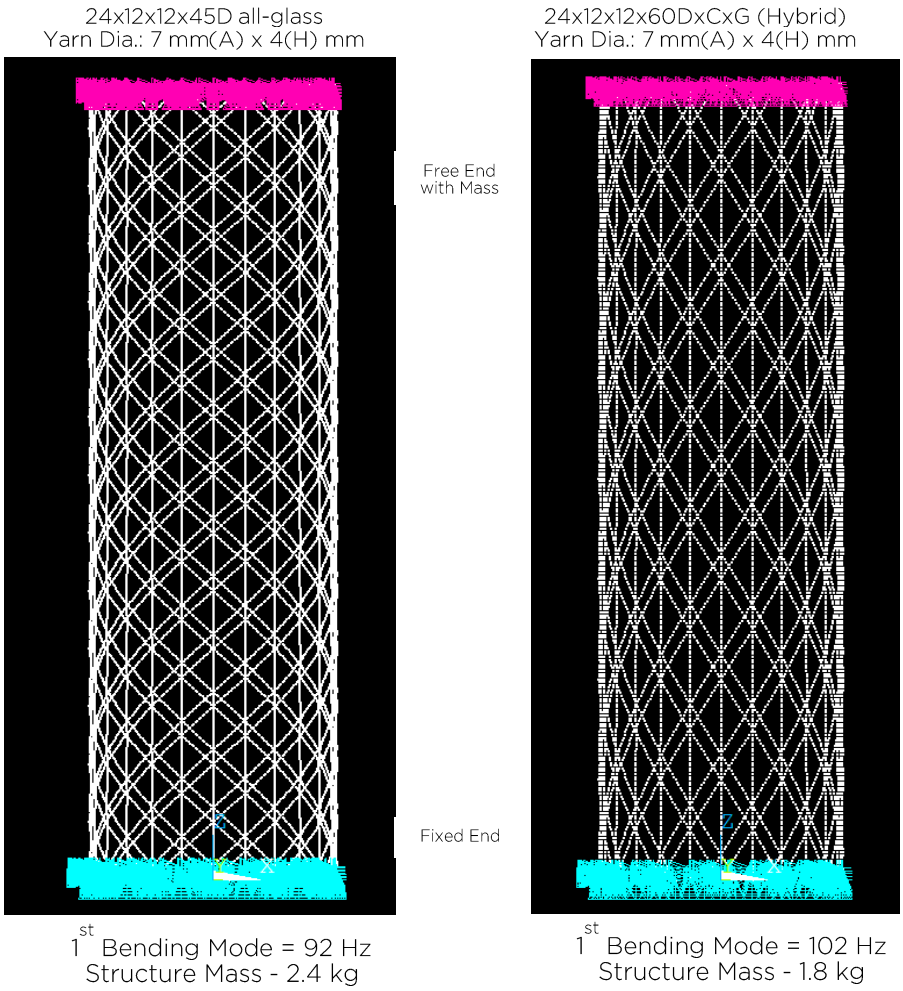

Figure 4.10: Modal Analysis of cantilevered cylindrical OACS – all - Glass and Hybrid

Figure 4.9 and Figure 4.10 show the wireframe models of the 250 mm diameter *x* 900 mm long all-carbon-fiber yarns OACS tubes in cantilevered boundary condition with an additional mass rigidly coupled to the nodes at the free end. The above tubes meet or are very close to meet the design requirement of 1st bending mode of greater than 100 Hz. "Openness" of the tubes is critical for RF transparency purposes, it refers to having minimal yarn coverage over the tube without losing-out on the overall stiffness of the structure. The figures help visualize the change in "openness" of the braided structure with changes in axial yarn count, helical yarn count and the helix angle.

Cylindrical OACS FE-Modal Analysis Results

Table 4.3: Cylindrical IROC OACS Modal results for 16x8x8

#	Material	Angle	Axial Dia. (mm)	Helical Dia. (mm)	Longest Span (mm)	Structure Mass (Kg.)	2kg 1st Mode (Hz.)	1.5kg 1st Mode (Hz.)
1	Glass	35	7	4	50	1.7	73	83
2	Glass	45	7	4	80	1.6	72	80
3	Carbon	45	7	4	80	1.1	109	122
4	Carbon	60	7	4	140	1	95	107

Table 4.4: Cylindrical IROC OACS Modal results for 16x16x16

#	Material	Angle	Axial Dia. (mm)	Helical Dia. (mm)	Longest Span (mm)	Structure Mass (Kg.)	2kg 1st Mode (Hz.)	1.5kg 1st Mode (Hz.)
1	Glass	45	7	4	30	2.14	80	89

Table 4.5: Cylindrical IROC OACS Modal results for 24x12x12

#	Material	Angle	Axial Dia. (mm)	Helical Dia. (mm)	Longest Span (mm)	Structure Mass (Kg.)	2kg 1st Mode (Hz.)	1.5kg 1st Mode (Hz.)
1	Glass	45	7	4	50	2.4	92	102.22
2	Glass	60	7	4	80	2.2	84	93

Table 4.6: Cylindrical IROC OACS Modal results for Hybrid tubes

SL. #	Axial Material and count	Helical Material and Yarn count (CW + CCW)	Angle in Deg.	Axial Dia. (mm)	Helical Dia. (mm)	Longest Span (mm)	Structure Mass (Kg.)	2kg 1st Mode (Hz.)
1	24 Carbon	24 Glass	60	7	4	80	1.8	101.95
2	48 Carbon	16 Glass	45	4	4	80	1.5	84
3	48 Carbon	24 Glass	45	4	4	50	1.6	89
4	48 Carbon	24 Glass	60	4	4	80	1.5	84

Table 4.7: Cylindrical IROC OACS Modal results for all carbon tube

SL #	Axial Material and Count	Helical Material and Count (CW+CCW)	Angle in Deg.	Axial Dia. (mm.)	Helical Dia. (mm.)	Axial yarn Span (mm.)	Structure Mass (Kg.)	2kg. 1st Mode (Hz.)	Gap Between axials (mm.)
1	16 Carbon	16 Carbon	45	7	4	80	1.1	109	42
2	16 Carbon	16 Carbon	60	7	4	140	1.0	95	42
3	32 Carbon	16 Carbon	45	4	4	85	0.8	84	12 and 32
4	48 Carbon	16 Carbon	45	4	4	85	1.1	105	32

The FE Modal analysis for the IROC OACS cylindrical tube with 250 mm diameter and 900 mm length indicates that a 16x8x8 all-carbon braid, with 7 mm axial yarn diameter - approximately 650K carbon filaments would be able to achieve the design requirement of exceeding 100 Hz., 1st bending mode. As of this period, due to manufacturing limitations, a yarn with 7 mm diameter cannot be braided due to limitations in effectively setting up the tow creels, braiding carrier bobbins and the braiding eyelets which are all crucial for achieving a high quality braided yarn.

The feasibility to braid a high-quality 4 mm diameter carbon fiber yarn with approximately 324K carbon filaments in the core led to the analysis of 48x8x8x45D all-carbon, 48x12x12x45D hybrid cylindrical OACS tubes, with an overall structural mass of around 1 Kg and 1.6 Kg respectively., significantly lower than the 2 Kg. overall structural mass design requirements.

As per the FE analysis, 48x8x8x45D all-carbon OACS tube with a 2 Kg. end mass (representing a mirror) exceeded the 100 Hz. minimum first lateral bending mode with a value of 105 Hz., and as of this period, Auburn University team was in the process of manufacturing the structure for experimental testing to correlate the FE results.

Hybrid OACS tubes with carbon axials and glass helicals might have higher RF transparency when compared to the all-carbon OACS tubes and hence FE modal analysis was performed to see if a hybrid combination would meet the design requirements. The 48x12x12x45D configuration with 4 mm diameter, 48 count carbon axials and 24 total count helicals

(CW+CCW) with 4 mm diameter glass-fiber yarns had a first lateral bending mode close to 90 Hz., design requirement being 100 Hz., it would be best to manufacture and test the hybrid braid to analyze and compare with the experimental results.

Conclusion

Multiple iterative models of the OACS tubes for IROC application were modelled and finite element modal analysis was performed to generate a comprehensive database for further analysis including RF testing and dynamic loading. Based on the ANSYS APDL FE code for modal analysis of the full-scale OACS tubes for IROC application, it was found that a 48x8x8x45D all-carbon OACS tube with 4 mm diameter yarns would be able to achieve 1st lateral bending mode exceeding 100 Hz.

Hybrid OACS tubes of 48x12x12x45D, with 4 mm diameter yarn architecture also showed promising results with 1st lateral bending frequency close to 100 Hz. The hybrid tubes with its glass-fiber helical yarns might have an advantage over the all-carbon tubes when tested for RF transparency and it is recommended to manufacture and experimentally test for validating the FE results.

Based of manufacturing feasibility and the packaging requirements which are to be considered further down in the research timeline, this work provides the researcher a list of suitable tube configurations to choose from.

Bibliography

[1] Gibson, R., Principles of Composite Material Mechanics

[2] Sangars, U., Development and Testing of Open Architecture Composite Structures and Composite Yarns for Compressive Strength, Master's Thesis, Auburn University, 2016

[3] Branscomb, D., Minimal Weight Composites Utilizing Advanced Manufacturing Techniques, Ph.D. Thesis, Auburn University, 2012.

[4] Gurley, A. Design and analysis of optimal braided composite lattice structures. Master's thesis, Auburn University, 2014.

[5] Roesler, J., Harders, H., Baeker. M., Mechanical Behavior of Engineering Materials

[6] Winkel, J., Dr. Akers, J., IROC PMC Woven Tube Modal Survey, Private Communication, NASA Glenn, February 2016

[7] Kothari, N., Mechanical Characterization of the Braided Composite Yarn and Bond Strength Evaluation of the Joints of the Open-Architecture Composite Structure (O-ACS), Auburn University, 2014

[8] Branscomb, D., Beale, D., and Broughton, R., New Directions in Braiding; Journal of Engineered Fibers and Fabrics, Accepted, 2012.

[9] Shirgaonkar, S., Development of Test Methods for Evaluation of Bending Stiffness and Compressive Modulus of Braided Composite Lattice Structures, Master's Thesis, Auburn University, December 2014.

[10] TCR Composites, Ogden, Utah, USA. Prepreg Resin Selector Guide, February 2014.

[11] Y. Shen, "Design, Processing, and Failure Analysis of Open-Architecture Composite Structures," Auburn University, Auburn, 2015.

[12] R. Broughton, D. Branscomb and D. Beale. United States Patent 8859088B2, 2014.

[13] 3M, "3M Scotch-Weld Epoxy Adhesive DP460," 2004.

[14] R. Lyman Ott, An Introduction to Statistical Methods and Data Analysis.

[15] ANSYS APDL Documentation, ANSYS, Inc.

[16] Gurley, A., Report on the Performance of the Conventional and Triaxial Braided Lattice, Private Communication, Auburn University, November 2014

[17] Mathworks.com/linear regression

[18] SAS.com/linear regression

[19] McEntire, K., Private Communication, NASA Glenn

Appendix

fell_point Matlab Parameters to Generate OACS Tube Coordinate Points

```
%% Structure Specification
% mandrel diameter
Dia = 0.25; %m (true diameter on round mandrel, max radius on polygons)
Dia2 = 0.25; %m (true diameter on round mandrel, max radius on polygons)

% pitch (length along z per wrap)
%pitch = 3*0.0254;
%h_angle = atan(pitch/(Dia*pi))*180/pi;

% helix angle (from wrapping direction!)
%h_angle = 35;
h_angle = 45;
%h_angle = 60;
pitch = tan(h_angle*pi/180)*(Dia*pi);
grade = 1.0; % scales the z sweep by t^grade

% number of wraps
%num_pats = 1+1/3;
%height = pitch*num_pats;

% structure height
 height = 0.9;
 num_pats = height/pitch;

% number of gear [ = (# axial ports), = (#carriers)/2]
num_ax =48;
% minor diameter (horn gear)
dia = (Dia*pi)/num_ax/2; %m
% minor diameter (FEA and visualization)
pdia = 0.006; %m
```

```
% warp loading (length = num_ax)
%warp = ones(1,num_ax);
%warp = zeros(1,num_ax);
warp = [1 0 0 0  0 0 1 0  0 0 0 0  1 0 0 0  0 0 1 0  0 0 0 0  1 0 0 0  0 0 1 0   0 0 0 0  1 0 0 0  0 0 1 0  0 0 0 0]; % 8 Helicals
% warp = [1 0 0 0  1 0 0 0  1 0 0 0  1 0 0 0  1 0 0 0  1 0 0 0  1 0 0 0  1 0 0 0   1 0 0 0  1 0 0 0  1 0 0 0  1 0 0 0]; % 12 Helicals
%warp = [1 1 1 1  1 0 0 0  1 0 0 0  1 0 0 0];
%warp = [1 0 1 0  1 0 1 0  1 0 1 0];
%d_warp = [d d d d d d d d];
%d_warp = d*ones(1,num_ax);
%d_warp = d*[1 .1 .1 .1  1 0 0 0  1 0 0 0  1 0 0 0];
d_warp = 0.0025*warp;
c_warp = {'r' 'r' 'r' 'r'  'r' 'r' 'r' 'r'  'r' 'r' 'r' 'r'  'r' 'r' 'r' 'r'  'r' 'r' 'r' 'r'  'r' 'r' 'r' 'r'  'r' 'r' 'r' 'r'  'r' 'r' 'r' 'r'  'r' 'r' 'r' 'r'  'r' 'r' 'r' 'r'  'r' 'r' 'r' 'r'  'r' 'r' 'r' 'r'  };

% weft loading (length = num_ax)
%weft = ones(1,num_ax);
%weft = zeros(1,num_ax);
%weft = [0 0 0 0 0  1 0 0 0  0 0 0 0  0 0 0 0  0 0 0 0  1 0 0 0  0 0 0 0  0 0 0 0  0 0 0 0   1 0 0 0  0 0 0 0  0 0 0 ];
weft = [0 1 0 0 0  0 0 1 0  0 0 0 0  1 0 0 0  0 0 1 0  0 0 0 0  1 0 0 0  0 0 1 0   0 0 0 0  1 0 0 0  0 0 1 0  0 0 0 ]; % 8 Helicals
% weft = [0 1 0 0 0  1 0 0 0  1 0 0 0  1 0 0 0  1 0 0 0  1 0 0 0  1 0 0 0  1 0 0 0   1 0 0 0  1 0 0 0  1 0 0 0  1 0 0 ]; % 12 Helicals
%weft = [1 1 1 1  1 0 0 0  1 0 0 0  1 0 0 0];
%weft = [0 1 0 1  0 1 0 1  0 1 0 1];
%d_weft = [d d d d  d d d d];
%d_weft = d*ones(1,num_ax);
%d_weft = d*[1 .1 .1 .1  1 0 0 0  1 0 0 0  1 0 0 0];
d_weft = 0.0025*weft;
%c_weft = {'r' 'r' 'r' 'r'  'r' 'r' 'r' 'r'  'r' 'r' 'r' 'r'  'r' 'r' 'r' 'r'};
c_weft = {'r' 'r' 'r' 'r'  'r' 'r' 'r' 'r'  'r' 'r' 'r' 'r'  'r' 'r' 'r' 'r'  'r' 'r' 'r' 'r'  'r' 'r' 'r' 'r'  'r' 'r' 'r' 'r'  'r' 'r' 'r' 'r'   'r' 'r' 'r' 'r'  'r' 'r' 'r' 'r'  'r' 'r' 'r' 'r'  'r' 'r' 'r' 'r' };

% axial loading (length = num_ax)
%axia = ones(1,num_ax);
%axia = zeros(1,num_ax);
%axia = [1 0 0 1  0 0 1 0  0 1 0 0  1 0 0 1  0 0 1 0  0 1 0 0  1 0 0 1  0 0 1 0   0 1 0 0  1 0 0 1  0 0 1 0  0 1 0 0];

%axia = [1 0 0 1  0 0 1 0  0 1 0 0  1 0 0 1  0 0 1 0  0 1 0 0  1 0 0 1  0 0 1 0   0 1 0 0  1 0 0 1  0 0 1 0  0 1 0 0];% 16 axials
 %axia = [1 0 1 0  1 0 1 0  1 0 1 0  1 0 1 0  1 0 1 0  1 0 1 0  1 0 1 0  1 0 1 0   1 0 1 0  1 0 1 0  1 0 1 0  1 0 1 0];% 24 axials
%axia = [1 1 0 1  1 0 1 1  0 1 1 0  1 1 0 1  1 0 1 1  0 1 1 0  1 1 0 1  1 0 1 1   0 1 1 0  1 1 0 1  1 0 1 1  0 1 1 0];% 32 axials
axia = [1 1 1 1  1 1 1 1  1 1 1 1  1 1 1 1  1 1 1 1  1 1 1 1  1 1 1 1  1 1 1 1   1 1 1 1  1 1 1 1  1 1 1 1  1 1 1 1];% 48 axials
```

Consolidating Generated Coordinate Points for ANSYS APDL

```
n = length(INFO.warp.X);
A = zeros(12*n,3);
count = 0;
for i = 1:1:48
    if isnan(INFO.warp.X(1,i)) == 0
        count = count+1;
        for j = 1:1:n
            A((count-1)*n+j,1) = INFO.warp.X(j,i);
            A((count-1)*n+j,2) = INFO.warp.Y(j,i);
            A((count-1)*n+j,3) = INFO.warp.Z(j,i);
        end
    end
end
for i = 1:1:48
    if isnan(INFO.weft.X(1,i)) == 0
        count = count+1;
        for j = 1:1:n
            A((count-1)*n+j,1)= INFO.weft.X(j,i);
            A((count-1)*n+j,2)= INFO.weft.Y(j,i);
            A((count-1)*n+j,3)= INFO.weft.Z(j,i);
        end
    end
end
for i = 1:1:48
    if isnan(INFO.axial.X(1,i)) == 0
        count = count+1;
        for j = 1:1:n
            A((count-1)*n+j,1) = INFO.axial.X(j,i);
            A((count-1)*n+j,2) = INFO.axial.Y(j,i);
            A((count-1)*n+j,3) = INFO.axial.Z(j,i);
        end
    end
end
```

ANSYS APDL FEA Input-File Generation Code

```
%% define line element for yarn
fprintf(fid,'*do,j,1,%f,1\n', number_of_warp);
fprintf(fid,'*do,i,1,%f,1\n', n-1);
fprintf(fid,'L,i+%f*(j-1),i+%f*(j-1)+1\n', n,n);
fprintf(fid,'*enddo\n');
fprintf(fid,'*enddo\n');

fprintf(fid,'*do,j,%f,%f,1\n', number_of_warp, p1);
fprintf(fid,'*do,i,1,%f,1\n', n-1);
fprintf(fid,'L,i+%f*(j-1),i+%f*(j-1)+1\n', n,n);
fprintf(fid,'*enddo\n');
fprintf(fid,'*enddo\n');

fprintf(fid,'*do,j,%f,%f,1\n', p1, number_of_yarn);%p2 for other cases
fprintf(fid,'*do,i,1,%f,1\n', n-1);
fprintf(fid,'L,i+%f*(j-1),i+%f*(j-1)+1\n', n,n);
fprintf(fid,'*enddo\n');
fprintf(fid,'*enddo\n');

GenCoordinateTaper_2mmElement();


% define line element for the joint
D1 = 2.8e-3^2;
D2 = 2.2e-3^2;
```

```
%% joints betw helicals and axials
number_of_joint = 0;
for h = number_of_warp+number_of_weft+1:1:number_of_yarn
    for k = 1:1:n
        for i=1:1:(number_of_warp+number_of_weft)*n
            if (A(i,1)-A((h-1)*n+k,1))^2+(A(i,2)-A((h-1)*n+k,2))^2+(A(i,3)-A((h-1)*n+k,3))^2 <= D1
                fprintf(fid,'L, %f, %f\n', i, (h-1)*n+k);
                number_of_joint = number_of_joint+1;
            end
        end
    end
end
%%
```

```
%Axial Yarns | Carbon
fprintf(fid,'et,1,beam188\n');
fprintf(fid,'MPTEMP,,,,,,,,\n');
fprintf(fid,'MPTEMP,1,0\n');
fprintf(fid,'mpdata,ex,1,,123.3e9\n');
fprintf(fid,'mpdata,ey,1,,7780e3\n');
fprintf(fid,'mpdata,ez,1,,7780e3\n');
fprintf(fid,'MPDATA,PRXY,1,,0.27\n');
fprintf(fid,'MPDATA,PRYZ,1,,0.4\n');
fprintf(fid,'MPDATA,PRXZ,1,,0.27\n');
fprintf(fid,'MPDATA,GXY,1,,5000e6,\n');
fprintf(fid,'MPDATA,GYZ,1,,3050e6,\n');
fprintf(fid,'MPDATA,GXZ,1,,5000e6\n');
fprintf(fid,'MPDATA,DENS,1,,1393\n');

fprintf(fid,'SECTYPE,1, BEAM, CSOLID, AxialY, 0\n');
fprintf(fid,'SECOFFSET, CENT\n');
fprintf(fid,'SECDATA,0.002,1,1,0,0,0,0,0,0,0,0,0\n');


% %Helical Yarns | Glass
% fprintf(fid,'et,2,beam188\n');
% fprintf(fid,'MPTEMP,,,,,,,,\n');
% fprintf(fid,'MPTEMP,1,0\n');
% fprintf(fid,'mpdata,ex,2,,5e9\n');
% fprintf(fid,'mpdata,ey,2,,8e9\n');
% fprintf(fid,'mpdata,ez,2,,8e9\n');
% fprintf(fid,'MPDATA,PRXY,2,,0.3\n');
% fprintf(fid,'MPDATA,PRYZ,2,,0.4\n');
% fprintf(fid,'MPDATA,PRXZ,2,,0.3\n');
% fprintf(fid,'MPDATA,GXY,2,,5e9,\n');
% fprintf(fid,'MPDATA,GYZ,2,,3.8462e9,\n');
% fprintf(fid,'MPDATA,GXZ,2,,5e9\n');
% fprintf(fid,'MPDATA,DENS,2,,2000\n');
%
% fprintf(fid,'SECTYPE,2, BEAM, CSOLID, HelicalY, 0\n');
% fprintf(fid,'SECOFFSET, CENT\n');
% fprintf(fid,'SECDATA,0.002,1,1,0,0,0,0,0,0,0,0,0\n');
```

Toray T700s Specification

COMPOSITE PROPERTIES*

Tensile Strength	370 ksi	2,550 MPa	ASTM D-3039
Tensile Modulus	20.0 Msi	135 GPa	ASTM D-3039
Tensile Strain	1.7 %	1.7 %	ASTM D-3039
Compressive Strength	215 ksi	1,470 MPa	ASTM D-695
Flexural Strength	245 ksi	1,670 MPa	ASTM D-790
Flexural Modulus	17.5 Msi	120 GPa	ASTM D-790
ILSS	13 ksi	9 kgf/mm^2	ASTM D-2344
90° Tensile Strength	10.0 ksi	69 MPa	ASTM D-3039

* Toray 250°F Epoxy Resin. Normalized to 60% fiber volume.

Toray T300 Specification

COMPOSITE PROPERTIES*

Tensile Strength	270 ksi	1,860 MPa	ASTM D-3039
Tensile Modulus	20.0 Msi	135 GPa	ASTM D-3039
Tensile Strain	1.3 %	1.3 %	ASTM D-3039
Compressive Strength	215 ksi	1,470 MPa	ASTM D-695
Flexural Strength	260 ksi	1,810 MPa	ASTM D-790
Flexural Modulus	18.0 Msi	125 GPa	ASTM D-790
ILSS	14 ksi	10 kgf/mm^2	ASTM D-2344
90° Tensile Strength	11.0 ksi	76 MPa	ASTM D-3039

* Toray 250°F Epoxy Resin. Normalized to 60% fiber volume.

Yarn #6 Specification Sheet

Auburn University
Advanced Braiding Lab
115 Textile Building
Auburn, AL 36849

Constituent Materials

	Material	Quantity	Size
True Triaxial Jacket			
CW Braider	Textured Nylon	4	500 D.
CCW Braider	Textured Nylon	4	500 D.
Axial	T300 Carbon	4	3K
Unidirectional Core			
Carbon	T700 Carbon	52% by volum	48K
Resin	UF3330	48% by volume	

Physical Properties

Property	Abbrev.	Units	Mean	Std. Dev.	Method
Maximum Diameter	D_max	mm	2.687	0.0615	
Minimum Diameter	D_min	mm	2.344	0.0674	
Effective Diameter	D_eff	mm	2.4	0.0526	
Effective Area	A	mm^2	4.524	0.0022	pi*D_eff^2/4
Effective Area Mol	I	mm^4	1.629	0.0000	pi*D_eff^4/64
Effective Polar Mol	J	mm^4	3.257	0.0000	pi*D_eff^4/32
Linear Density	Rho_linear	g/m	6.3		4 m length

Stiffness

Property	Abbrev.	Units	Mean	Std. Dev.	Method
Axial Stiffness	AE	kN	482.89	38.5600	Potted w/ resin in steel pipe
Axial Modulus*	E	GPa	106.74		E=AE/A
Flexural Stiffness	EI	Nm^2	0.0676	0.00197	3 point, 40mm span
Flexural Modulus*	E_flex	GPa	41.51		E=EI/I
Short-Beam Shear Stiffne	AG	kN/m	408.9700		Short-beam shear, 10 mm spar
Beam Shear Modulus*	G1	GPa	45.20		G=AG/2A
Torsional Stiffness	JG	Nm^2	0.0034	0.00056	NASA torsion fixture
Torsion Shear Modulus*	G2	MPa	1053.05		G=JG/J

Strength

Property	Abbrev.	Units	Mean	Std. Dev.	Method
Tensile Breaking Load	L_tensile	N	7494.00	175	Potted w/ resin in steel pipe
Tensile Strength*	S_tensile	MPa	1656.54		sigma=P/A
Compressive Breaking Loa	_compressior	N	2542.12	145.9	pinned, 7 mm gauge
Compressive Strength*	S_compressive	MPa	581.14		sigma=P/A
Flexural Breaking Load	L_bending	Nm	1.51	0.0956	3 Pt., 40mm span
Flexural Strength*	S_bending	MPa	1112.17		sigma=M*(D_eff/2)/I
Torsional Breaking Load	L_shear	Nm	0.12	0.0056	1" Gage length, 5 Samples
Shear Strength*	S_shear	MPa	43.73		tau=T*(D_eff/2)/J

Bonded Joint

Property	Abbrev.	Units	Mean	Std. Dev.	Method
Radial Seperation	S_joint_norma	N	86.298	1.664	Hook fixture using string
Slipping Shear	S_joint_shear	N	191.35	66.44	Hook fixture using blocks

OACS Tubes End Caps for 44.5 mm Diameter x 300 mm Long